

# UniCorrn: Unified Correspondence Transformer Across 2D and 3D

Prajnan Goswami<sup>1\*</sup> Tianye Ding<sup>1\*</sup> Feng Liu<sup>2</sup> Huaizu Jiang<sup>1</sup>  
<sup>1</sup>Northeastern University <sup>2</sup>Adobe Research

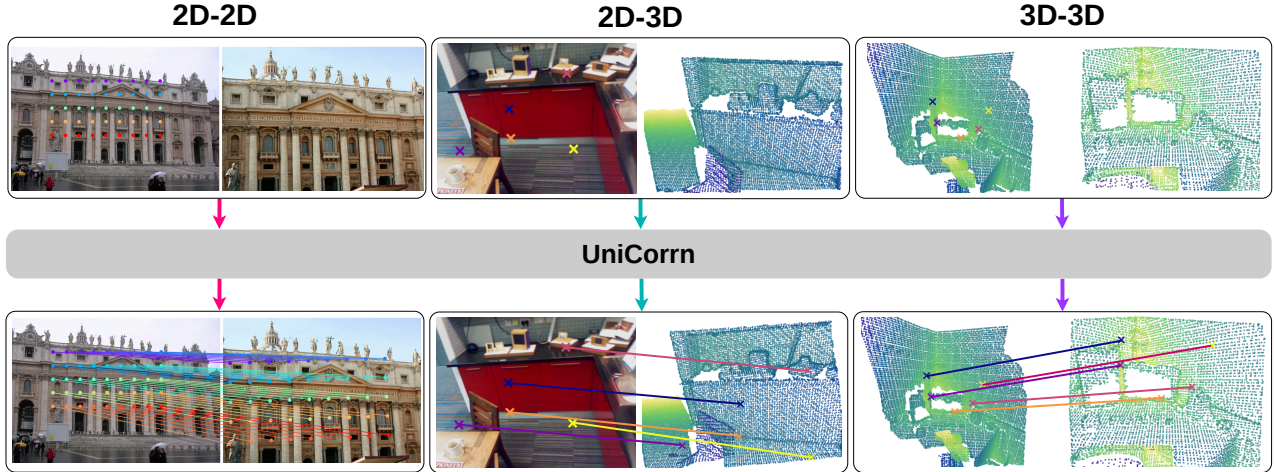


Figure 1. **UniCorrn** is a unified correspondence transformer that can find correspondences of keypoints of interest across 2D and 3D.

## Abstract

Visual correspondence across image-to-image (2D-2D), image-to-point cloud (2D-3D), and point cloud-to-point cloud (3D-3D) geometric matching forms the foundation for numerous 3D vision tasks. Despite sharing a similar problem structure, current methods use task-specific designs with separate models for each modality combination. We present **UniCorrn**, the first correspondence model with shared weights that unifies geometric matching across all three tasks. Our key insight is that Transformer attention naturally captures cross-modal feature similarity. We propose a dual-stream decoder that maintains separate appearance and positional feature streams. This design enables end-to-end learning through stack-able layers while supporting flexible query-based correspondence estimation across heterogeneous modalities. Our architecture employs modality-specific backbones followed by shared encoder and decoder components, trained jointly on diverse data combining pseudo point clouds from depth maps with real 3D correspondence annotations. **UniCorrn** achieves competitive performance on 2D-2D matching and surpasses prior state-of-the-art by 8% on 7Scenes (2D-3D) and 10% on 3DLoMatch (3D-3D) in registration recall. Project website: [neu-vi.github.io/UniCorrn/](https://neu-vi.github.io/UniCorrn/)

## 1. Introduction

Visual correspondence, the task of finding matching features across different observations of the same scene, plays a fundamental role in 3D computer vision. Geometric keypoint matching can be categorized into three types: image-to-image (2D-2D), image-to-point cloud (2D-3D), and point cloud-to-point cloud (3D-3D) matching, as shown in Figure 1. These inter-modal and intra-modal keypoint matches form the foundation for various downstream applications, including point cloud registration [22], camera pose estimation [15], structure from motion and SLAM [4, 65].

Although significant advances have been made in solving various forms of visual correspondence problems, different specialist models maintain different task-specific designs [8, 18, 25, 33, 48, 55] despite the similar nature of the problem across 2D and 3D domains. While some works have explored unified matching within the 2D image domain [10, 23, 59, 75, 84, 86], no solution exists for geometric correspondence across 2D and 3D modalities. In this paper, we ask: *is it possible to approach geometric matching across 2D and 3D modalities using a unified model?* A unified correspondence model not only represents a grand scientific pursuit toward general-purpose visual perception, but also has the potential to enable seamless cross-modal reconstruction pipelines, reduce engineering complexity, and facilitate learning of shared geometric priors across modalities through joint training.

\* Equal contribution

Addressing this question requires overcoming fundamental methodology limitations in existing 2D unification approaches that prevent their extension to 3D domains. These efforts can be broadly grouped into three categories, each with distinct architectural constraints. First, cost volume-based methods [23, 59, 84] capture feature similarity within local ranges to ensure efficiency, from which coarse-to-fine estimations are performed via image pyramids or recurrent networks. However, the fixed depth of pyramids or sequential nature of recurrent operations limits their representational capacity, making them unsuitable for handling the sparse and irregular structure of 3D point clouds where correspondences may span large spatial distances. Second, nearest-neighbor (NN) search methods [10, 75] match dense feature descriptors, but NN search can only be performed once and cannot be incorporated into stacked neural network layers for end-to-end training. This prevents iterative feature refinement necessary for learning robust cross-modality alignments between heterogeneous 2D and 3D representations. Third, while direct regression approaches [86] fuse image features with transformers and directly regress dense pixel displacements, our experiments show that direct regression struggles in 2D-3D and 3D-3D settings where explicit geometric reasoning about 3D structure is essential for accurate correspondence estimation. These limitations motivate our approach: we need a matching mechanism that (1) supports end-to-end learning through stackable layers, (2) handles irregular structures across modalities, and (3) enables iterative geometric refinement of correspondence estimation.

In this paper, we present **UniCorrn**, a unified correspondence model based on the Transformer architecture [62] that addresses geometric matching tasks across 2D-2D, 2D-3D, and 3D-3D modalities. Our key insight is that attention mechanism in Transformers naturally captures feature similarity, which is the essence of correspondence across all modalities. To effectively leverage this property for cross-modal matching, we develop a novel dual-stream attention mechanism in our matching decoder, where we maintain separate residual streams for appearance and positional features. These streams are combined to compute attention maps, based on which both appearance and positional features are updated independently. This design enables us to regress matching keypoint locations from attention-modulated positional encodings while supporting end-to-end learning through stacked Transformer layers. Crucially, our model employs modality-specific backbones followed by a shared feature fusion encoder and matching decoder with identical weights across all input modality combinations. This weight-sharing design, as opposed to training separate models for each task, enables joint learning of geometric priors across 2D and 3D domains. Given source keypoints of interest, our model directly decodes their corre-

sponding locations in the target modality, providing a flexible query-based interface for correspondence estimation.

Inspired by recent foundation models for computer vision [29, 31, 45, 66, 69], we train our unified model on diverse correspondence data across modalities. We leverage pretrained CroCo v2 [69] for image feature extraction and build our correspondence model with 600M parameters, enabling rich representation learning while maintaining computational efficiency. A key challenge is the scarcity of training data for 2D-3D and 3D-3D correspondences compared to abundant 2D-2D image pairs. To address this, we combine pseudo point-cloud data derived from depth maps used in DUST3R training [67] with smaller amounts of high-quality 3D correspondence annotations [1, 47, 83]. This mixed training strategy enables our model to learn robust geometric priors across modalities. Experimental results show that UniCorrn achieves competitive performance in 2D-2D matching and surpasses existing methods in 2D-3D by 8% and 3D-3D by 10% in registration recall on standard benchmarks. Extensive ablation studies further validate the effectiveness of our model design, especially the dual-stream matching decoder.

In summary, we make three major contributions:

- We present UniCorrn, the first unified correspondence model with shared weights for geometric matching across 2D-2D, 2D-3D, and 3D-3D modalities.
- We propose a novel dual-stream Transformer decoder that decouples appearance and positional features, enabling stackable layers for correspondence matching.
- We achieve state-of-the-art results on 7Scenes [21] (2D-3D) and 3DLoMatch [83] (3D-3D) correspondence, surpassing prior methods by 8% and 10% in registration recall respectively, while maintaining competitive performance on 2D-2D matching.

## 2. Related Work

**Image to image (2D-2D).** In 2D-2D matching, learning-based methods include keypoint detection, feature description extraction, and feature matching [12, 41, 50, 52, 60]. Recent methods [7, 18, 19, 31, 55] have replaced keypoint detection with detection-free approach. These methods perform dense matching by feature warping for spatial alignment [18, 19, 23, 44, 59] or by computing similarity between features followed by nearest neighbor search [31, 55, 68, 75, 81]. COTR [26] and VGGT [66] allow users to query keypoints on one image and directly estimate the correspondences on the other. The query method is commonly used in video key-point tracking tasks [13, 14, 28, 66], however, it is underexplored for geometric matching.

**Image to point cloud (2D-3D).** To predict correspondences between images and point clouds, seminal deep learning methods [20, 47] directly match pairs of learned local image patch and local point cloud volume descriptors with

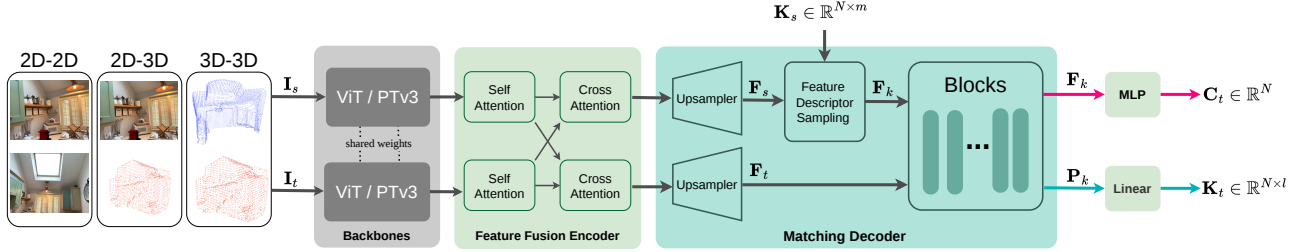


Figure 2. **Illustration of the overall architecture design.** Our model consists of four main modules: (1) modality-specific backbone, (2) feature fusion encoder, (3) matching decoder, and (4) modality-specific prediction heads. Details of each module can be found in Sec. 3.1.

a distance metric. For dense per-pixel/per-point correspondences, DeepI2P [32] classifies whether each point in the point cloud lies within or beyond the camera frustum. Recent work [8, 27, 33, 63] achieves better matching with circle loss [57] and adopts a coarse-to-fine matching strategy. FreeReg [64] and DiffReg [70] incorporate diffusion [24] into the matching pipeline, improving cross-modality matching at the cost of diffusion sampling time.

**Point cloud to point cloud (3D-3D).** Learning-based 3D-3D methods can be broadly classified into matching with 3D local descriptors and point-cloud registration. Early work [1, 25, 83] extracts local 3D patch descriptors and estimates 3D-3D correspondences by computing per-point overlap and matching scores. Recent state-of-the-art methods [34, 48, 78, 80, 82] use Transformer [62] with cross-attention to enhance 3D superpoint features. These methods directly supervise the model on rigid SE(3) transformation to avoid the high computation cost of matching dense feature descriptors.

**Unified correspondence models.** Unified correspondence models aims to solve more than one correspondence tasks. UCN [10] supervises CNN feature maps between image pairs with contrastive loss and uses nearest neighbor search to estimate geometric and semantic correspondences. Glu-Net [59] unifies geometric, semantic, and optical flow by computing similarity for across feature pyramids. RGM [84] proposes a two-stage model with iterative refinement for dense flow and sparse geometric matching. MatchAnything [23] supervises existing 2D-2D matching methods [19, 68] with large-scale data containing multiple imaging modalities such as thermal, tomography, histology, etc. MATCHA [75] incorporates features extracted from foundational models, Stable Diffusion [51] and DINOv2 [45], to unify matching across geometric, semantic and temporal keypoint tracking. UFM [86] fuses image features with a global attention Transformer and directly regresses the enhanced features for 2D-2D geometric and temporal matching.

### 3. Method

The input to our model consists of  $\mathbf{I}_s, \mathbf{I}_t$  and a list of keypoints of interest  $\mathbf{K}_s \in \mathbb{R}^{N \times m}$  in  $\mathbf{I}_s$ , where  $\mathbf{I}_s$  and  $\mathbf{I}_t$  represent the input source and target modalities, respectively.  $m \in \{2, 3\}$  indicates the modality dimension depending on the task specification. The source and target pair  $\mathbf{I}_s, \mathbf{I}_t$  can be formed between image-to-image (2D-2D), image-to-point (2D-3D), and point-to-point (3D-3D). The keypoints  $\mathbf{K}_s$  can be either from a detector [12, 39, 87] or sampled from an equally spaced grid. The output are a set of matching keypoints  $\mathbf{K}_t \in \mathbb{R}^{N \times l}$  in the target  $\mathbf{I}_t$  with  $l \in \{2, 3\}$  depending on the modality of  $\mathbf{I}_t$ , and confidence scores  $\mathbf{C}_t \in \mathbb{R}^N$ . The confidence scores quantifies the model’s uncertainty in matching keypoints in challenging areas like occluded regions, translucent objects, sky, etc.

#### 3.1. Network Architecture

We design a unified correspondence model based on Transformer [62] following recent large-scale models [31, 66, 67, 69] in 3D computer vision. As shown in Fig. 2, our model consists of four main modules: (1) modality-specific backbone, (2) feature fusion encoder, (3) matching decoder, and (4) modality-specific prediction head.

**Modality-specific backbones.** We use separate feature extractors for images and point clouds. Specifically, we use a ViT [17] for 2D images and Point Transformer v3 (PTv3) [72] for 3D point clouds. ViT and PTv3 have shown state-of-the-art performance in various computer vision tasks, thereby making them a good choice for our unified correspondence Transformer model. The backbone weights are shared in a Siamese manner when both source  $\mathbf{I}_s$  and target  $\mathbf{I}_t$  belong to the same modality. Rotary position embeddings [54] are used to encode relative positional information for both image and point cloud tokens.

**Feature fusion encoder.** We do not assume any modality specifics at this stage. The feature fusion encoder takes as input the modality-specific features of  $\mathbf{I}_s$  and  $\mathbf{I}_t$ . We use a generic design here following existing matching frameworks [22, 33, 55, 69] to allow information exchange between the input via cross-attention. Each encoder block has alternating layers of self-attention, where each token attends

to all tokens of the same input, and cross-attention, where each token attends to all tokens of the other input.

**Matching decoder.** Our main contribution is the Transformer-based matching decoder, where we propose a novel dual-stream attention module for keypoints matching. First, the fused image features from the output of the feature fusion encoder are upsampled using an MLP with Pixel Shuffle [53], and a PTv3’s learned upsampler [72] is used for fused point features. The upsampled features corresponding to the *source* and *target* inputs are indicated by  $\mathbf{F}_s$  and  $\mathbf{F}_t$ , respectively. Along with keypoints-of-interest of the *source* input  $\mathbf{K}_s$ , they are processed by a set of dual-stream Transformer layers, outputting a positional embedding  $\mathbf{P}_k$  and appearance feature  $\mathbf{F}_k$ , which contain useful feature representations for regressing correspondences in the target and estimating the uncertainties, respectively. We will introduce this module with more details in Sec. 3.2.

**Prediction heads.** The positional embedding  $\mathbf{P}_k$  from the matching decoder is fed into modality-specific linear layers to regress the 2D or 3D coordinates  $\mathbf{K}_t$  of corresponding keypoints. And a shared MLP takes as input the updated keypoint features  $\mathbf{F}_k$  from the matching decoder and predicts confidence scores  $\mathbf{C}_t$  for the correspondences.

### 3.2. Matching Decoder

**Encoding keypoints of interest.** Given the keypoints of interest  $\mathbf{K}_s$ , we obtain keypoint descriptors, denoted as  $\mathbf{F}_k$ , from  $\mathbf{F}_s$  using bilinear interpolation if  $\mathbf{I}_s$  is an image. If it is a point cloud, a shared Gaussian distribution with a learnable  $\sigma$  is applied to produce a single weighted feature vector from k-nearest features of each 3D keypoint.

**Capturing similarity via attention in Transformer.** The essence of various correspondence tasks by definition is to capture the similarity between  $\mathbf{F}_k$  and  $\mathbf{F}_t$ . Our core insight of designing the matching decoder is that the attention matrix in a Transformer layer captures the **matching cost** between the input pair, *i.e.*, correlation between two inputs in existing correspondence tasks [16, 22, 33, 55]. Specifically, we first compute position-augmented features

$$\mathbf{F}'_k = \text{RoPE}(\mathbf{F}_k \mathbf{W}_Q, \mathbf{K}_t), \quad \mathbf{F}'_t = \text{RoPE}(\mathbf{F}_t \mathbf{W}_K, \mathbf{X}_t),$$

where  $\text{RoPE}$  represents rotary position embedding [54].  $\mathbf{X}_t$  are the coordinates of the tokens in  $\mathbf{F}_t$ .  $\mathbf{K}_t$  are the estimated coordinates of corresponding keypoints according to Eq.(6) below.  $\mathbf{W}_Q$  and  $\mathbf{W}_K$  are the weight matrices associated with the query and key in Transformer, respectively. The attention matrix is then computed as

$$\mathbf{A} = \text{Softmax} \left( \frac{\mathbf{F}'_k \mathbf{F}'_t{}^T}{\sqrt{D}} \right), \quad (1)$$

where  $D$  is the feature dimension. This attention matrix  $\mathbf{A}$  is similar to the normalized version of the learnable cost

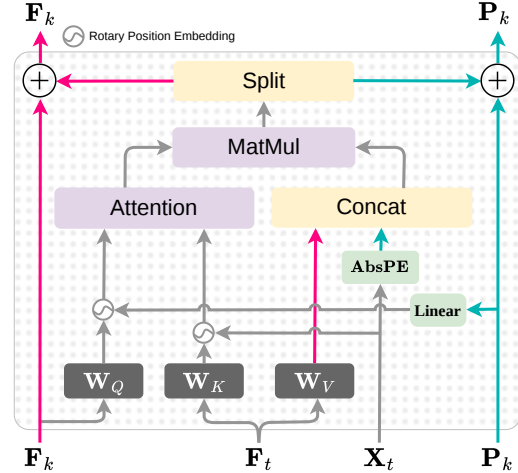


Figure 3. **Dual-stream attention with a single attention matrix (matching cost).** The appearance and position features are concatenated along the channel dimension to process them in parallel. After applying attention, the output is split to update the corresponding *appearance*  $\mathbf{F}_k$  and *positional*  $\mathbf{P}_k$  residual streams.

volume studied in [74]. In an ideal case with perfect similarity scores, each row in  $\mathbf{A}$  is a one-hot vector, where the position of 1 corresponds to the correct matching keypoint. A Transformer layer then works as<sup>1</sup>

$$\mathbf{Q} = \mathbf{A} \mathbf{V} + \mathbf{Q}. \quad (2)$$

Here  $\mathbf{Q}$  and  $\mathbf{V}$  denote the query and value vector in a Transformer in general. If we set  $\mathbf{V}$  to the *absolute positional encoding* of every pixel in  $\mathbf{I}_t$ , the updated query  $\mathbf{Q}$  contains the positional encoding of the correct corresponding pixels for every keypoint in  $\mathbf{K}_s$ , from which we can regress the coordinates. *The readers are highly encouraged to check an illustration provided in the supplementary material.*

**Dual-stream Transformer design.** The power of the Transformer design lies in that multiple Transformer layers can be stacked to refine the input, where the output of one layer will be used as input to the next layer. It is not feasible, however, to directly stack multiple Transformer layers introduced in Eq.(2) as the output  $\mathbf{Q}$  consists of *positional encoding only*, which cannot be used to match the appearance features  $\mathbf{F}_k$  in subsequent Transformer layers. To overcome this issue, we propose a dual-stream design for a Transformer layer by separating the appearance and positional embeddings. An illustration is shown in Fig. 3. Our ablation study shows that it works better than other instantiations of Transformer for visual correspondences [26, 86]. First,  $\mathbf{F}_k$  is updated in the first stream as

$$\mathbf{F}_k = \mathbf{A}(\mathbf{W}_V \mathbf{F}_t) + \mathbf{F}_k. \quad (3)$$

<sup>1</sup>We omit module such as FFN, LayerNorm, here for brevity.

Second, we introduce the other stream with a positional embedding  $\mathbf{P}_k$ , defined as

$$\mathbf{P}_k = \mathbf{A}(\text{AbsPE}(\mathbf{X}_t)) + \mathbf{P}_k, \quad (4)$$

where  $\text{AbsPE}(\mathbf{X}_t) = \mathbf{W}_p \mathbf{X}_t + \mathbf{b}_p$  indicates a learned *bijective* absolute positional encoding with parameters  $\mathbf{W}_p$  and  $\mathbf{b}_p$ . The positional embedding  $\mathbf{P}_k \in \mathbb{R}^{N \times D}$  is initialized with zeros. Similar to how the appearance features  $\mathbf{F}_k$  is updated in Eq.(3), here the positional embeddings is updated separately. Note that both the appearance features and positional embeddings will still be combined to compute the attention matrix  $\mathbf{A}$ . In practice, we replace the vanilla attention in Eq.(1) with a Gaussian variant

$$\mathbf{A} = \text{Softmax} \left( -\frac{\text{Pair\_L2}(\mathbf{F}'_k, \mathbf{F}'_t)}{D} \right), \quad (5)$$

where  $\text{Pair\_L2}$  computes the pairwise L2 distance. The vanilla attention matrix can be interpreted as using a linear kernel to compute the feature similarities between query and key, which only capture linear correlations and are sensitive to the scales of the magnitude of features. Similar to matching through descriptors [3, 40], we use a Gaussian kernel to capture the non-linear complex correlations. Experimental results show that it works better.

**Regressing the coordinates of correspondences.** With the output positional embedding  $\mathbf{P}_k$ , we can directly regress the coordinates of the corresponding keypoints  $\mathbf{K}_t$  using a linear layer as

$$\mathbf{K}_t = \mathbf{W}_p^+(\mathbf{P}_k - \mathbf{b}_p), \quad (6)$$

where  $\mathbf{W}_p^+$  is the Moore–Penrose inverse [43, 46] of  $\mathbf{W}_p$ . We also estimate pixel-wise confidence scores  $\mathbf{C}_t$  for the output correspondences using a shared MLP for all modalities that takes  $\mathbf{F}_k$  as input.

**Stacking dual-stream Transformer layers.** By decomposing the appearance features  $\mathbf{F}_k$  and positional embeddings  $\mathbf{P}_k$  into two separate streams, we can stack multiple such Transformer layers together, where the updated  $\mathbf{F}_k$  and  $\mathbf{P}_k$  of the current layer will be fed into the subsequent layer. As a result, by stacking multiple layers together, both  $\mathbf{F}_k$  and  $\mathbf{P}_k$  will be gradually refined, leading to more accurate attention matrices and thus more accurate correspondence estimation.

### 3.3. Training Objective

Our model is supervised with a loss for jointly training all three tasks

$$\mathcal{L}_{total} = \mathcal{L}_{2d2d} + \mathcal{L}_{2d3d} + \mathcal{L}_{3d3d}. \quad (7)$$

For each task, we consider the following three objectives

$$\mathcal{L}_{task} = \mathcal{L}_{conf} + \mathcal{L}_{aux} + \beta \mathcal{L}_{desc}, \quad (8)$$

where  $task \in \{2d2d, 2d3d, 3d3d\}$ .  $\beta$  is a weight to balance the loss terms. The three losses are introduced below.

**Confidence-aware L1 Loss.** The model is directly supervised with the error of the predicted keypoints using L1 loss. To quantify the uncertainty of predictions in parts of the input such as sky, occluded objects, etc., we incorporate the confidence-aware loss adapted from MAST3R [31].

$$\mathcal{L}_{conf} = \frac{1}{N} \sum_{i=1}^N \mathbf{C}_t(i) \|\mathbf{K}_t(i) - \bar{\mathbf{K}}_t(i)\|_1 - \alpha \log \mathbf{C}_t(i),$$

where  $\bar{\mathbf{K}}_t$  denote the ground-truth coordinates of corresponding keypoints.  $\alpha$  is a regularization strength.

**Contrastive loss.** We supervise the input features to have one-to-one correspondences using the InfoNCE loss [61], which helps improve the attention matrix. Specifically, we use ground-truth correspondence pairs to extract feature descriptors  $\mathbf{F}_s^{desc}$  and  $\mathbf{F}_t^{desc}$  from the upsampled fused features  $\mathbf{F}_s$  and  $\mathbf{F}_t$ , respectively. We then compute the InfoNCE loss ( $\mathcal{L}_c$ ) between these descriptors, and also apply the same loss to the output of the matching decoder  $\mathbf{F}_k$  and the extracted *target* features  $\mathbf{F}_t^{desc}$ .

$$\mathcal{L}_{desc} = \mathcal{L}_c(\mathbf{F}_s^{desc}, \mathbf{F}_t^{desc}) + \mathcal{L}_c(\mathbf{F}_k, \mathbf{F}_t^{desc}). \quad (9)$$

Details are provided in the supplementary material.

**Auxiliary supervision.** We also estimate the coordinates of corresponding keypoints at each of the matching decoder layer to provide auxiliary supervision. Let  $\mathbf{K}_t^{(l)}$  denote the estimated coordinates at the  $l$ -th decoder layer. The auxiliary loss is defined as

$$\mathcal{L}_{aux} = \sum_{l=1}^L \gamma^{L-l} \frac{1}{N} \sum_{i=1}^N \|\mathbf{K}_t^{(l)}(i) - \bar{\mathbf{K}}_t(i)\|_1, \quad (10)$$

where  $L$  is the total number of matching decoder layers and  $\gamma$  is a coefficient set to 0.9.

## 4. Experiments

### 4.1. Setup

**Datasets.** We train our unified model on the 2D-2D task with 7 datasets: ARKitScenes [2], BlendedMVS [76], CO3D-v2 [49], MegaDepth [36], StaticThings3D [42], ScanNet++ [77] and Waymo [56]. For the 2D-3D task, we use 7Scenes [21] and RGB-D Scenes v2 [30]. And finally for the 3D-3D, 3DMatch [83] and ModelNet [73] are used. We complement the 2D-3D and 3D-3D datasets with pseudo data generated from the dense depth maps of ScanNet++ [77] and ARKITScenes [2].

**Evaluation protocols.** To measure the performance of 2D-2D, we report the *Area Under Curve* (AUC) of the relative pose errors at 5°, 10° and 20° degree thresholds following

Table 1. **Ablation of different matching paradigms on single task small-scale experiments.** The top two methods represent *dense matching* design and the bottom four rows represent *key-point queryable* design.

Matching Paradigm	MegaDepth (2D-2D)		7Scenes (2D-3D)		3DMatch (3D-3D)	
	5° ↑	10° ↑	IR ↑	RR ↑	IR ↑	RR ↑
Nearest neighbor	49.8	<b>67.1</b>	42.0	63.4	24.8	87.5
Global matching	48.8	64.9	65.2	75.8	<b>93.1</b>	96.5
Regression	0.2	1.5	10.0	17.0	5.7	18.2
Sequence concatenation	10.3	22.1	12.8	21.1	2.4	7.3
Ours	<b>50.6</b>	<b>67.1</b>	<b>66.3</b>	<b>77.8</b>	92.8	<b>96.9</b>

Table 2. **Ablation of different design choices.** We analyze the impact of our contributions in the query matching decoder with detailed explanations provided in Section 4.2.  $D$  and  $H$  refers to embedding dimensions and number of attention heads.

Setup	MegaDepth-1500		
	5° ↑	10° ↑	20° ↑
I (Baseline): $D = 256, H = 16$	36.4	53.9	68.9
II: I, Gaussian Attention	37.3	54.7	69.5
III: II, 800 Keypoint Queries	38.2	55.8	70.7
IV: III, $D = 256, H = 1$	39.5	57.0	71.3
V: IV, Contrastive Loss	43.9	60.7	74.5
VI: V, $4\times$ Upscale, $D = 64, H = 1$	48.5	65.1	77.9
<b>VII (Final): VI, <math>D = 256, H = 1</math></b>	<b>50.6</b>	<b>67.1</b>	<b>79.6</b>

the evaluation protocol in [7, 52, 55]. The pose error is defined as the maximum of angular errors in rotation and translation. For 2D-3D and 3D-3D, we follow the evaluation protocol in [33] and [25, 78], respectively. Specifically, we report: (1) *Inlier Ratio* (IR), the ratio of pixel-to-point or point-to-point matches whose 3D distance is below a certain threshold over all putative matches; (2) *Feature Matching Recall* (FMR), the ratio of 2D-2D or 3D-3D pairs whose IR is above a certain threshold; (3) *Registration Recall* (RR), the ratio of 2D-3D or 3D-3D pairs whose RMSE is below a certain threshold. Additionally, we report the registration pose errors as *Relative Rotation Error* (RRE) and *Relative Translation Error* (RTE) on 3DMatch [83] and ModelNet [73].

**Implementation details.** We train two models with different capacities. A small-scale model is employed for the ablation study in Section 4.2, and a scaled up version for the benchmark in Section 4.3. The large-scale model is trained in two stages. Complete architectural details and training schemes are available in the supplementary materials.

## 4.2. Ablation Study

**Methods for estimating correspondences.** We first study the effectiveness of our proposed dual-stream matching decoder across 2D-2D, 2D-3D and 3D-3D correspondence

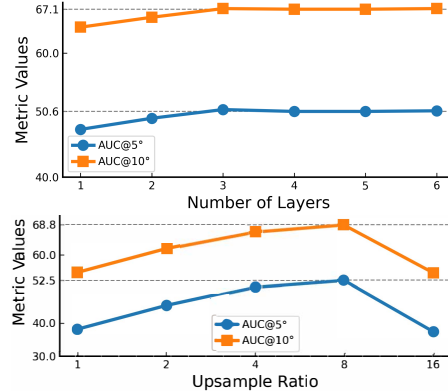


Figure 4. **Top:** AUC vs. number of matching decoder layers. **Bottom:** AUC vs. feature upsampling ratio. The results are obtained on the MegaDepth-1500 dataset.

tasks in Table 1. We compare our design to four alternative commonly adopted matching paradigms using the same small-scale model but replacing our matching decoder with *nearest neighbor*, *global matching* (similar to [31, 85]), *regression* (similar to [69, 86]) and *sequence concatenation* (similar to COTR [26]). As shown in Table 1, the regression and sequence concatenation methods show the worst results across all tasks. Nearest neighbor matching with dense features underperform on 2D-3D and 3D-3D tasks compared to our approach. While *global matching* achieves comparable results to our method, it is computationally expensive as it relies on large (full) feature resolution and takes approximately  $2\times$  the training duration compared to our method.

We further ablate different design choices for our model, where we *progressively* add different components. The results are summarized in Table 2. Starting with Setup I (baseline), the model has 8 matching decoder layers, 16 attention heads ( $H = 16$ ), vanilla attention,  $D = 256$ , and no feature upsampling. It is trained for 30 epochs on the MegaDepth dataset using 100 keypoint queries and 68,400 2D-2D samples per epoch. We make the following ablations. Setup II replaces vanilla attention with Gaussian attention, leading to better results. Setup III increases keypoint queries per training sample from 100 to 800 to supervise the model, showing improved accuracy. Recognizing that single-head attention approximates nearest neighbor matching, Setup IV tests this approach showing further performance improvements. Setup V adds contrastive loss supervision, improving feature descriptor quality. Setup VI upsamples spatial resolution by  $4\times$  using MLP with Pixel Shuffle [53], leading to great improvement in accuracy. Finally, Setup VII keeps the embedding dimension  $D = 256$  after upsampling. This represents our chosen configuration for the final model.

We further investigate the small-scale model from Setup VII with different number of decoder layers and feature upsampling ratios. As can be seen in Fig. 4, our match-

Table 3. **Image-to-Image (2D-2D) matching comparison on MegaDepth-1500 and ScanNet-1500.** Gray text indicates ScanNet [11] was part of the training datasets. **Bold** and underline highlights best and second best results.

Methods	AUC@ →	MegaDepth-1500			ScanNet-1500		
		5° ↑	10° ↑	20° ↑	5° ↑	10° ↑	20° ↑
SP + SG [12, 52]		49.7	67.1	80.6	16.2	32.8	49.7
SP + LG [12, 37]		51.0	68.1	80.7	14.8	30.8	47.5
LoFTR [55]		52.8	69.2	81.2	16.9	33.6	50.6
Efficient LoFTR [68]		56.4	72.2	83.5	19.2	37.0	53.6
ASpanFormer [7]		55.3	71.5	83.1	19.6	37.7	54.4
DKM [18]		<u>60.4</u>	<u>74.9</u>	<u>85.1</u>	26.6	47.1	64.2
RoMa [19]		<b>62.6</b>	<b>76.7</b>	<b>86.3</b>	28.9	50.4	68.3
MASt3R [31]		53.1	70.0	82.4	<u>34.1</u>	<u>57.1</u>	<u>74.3</u>
VGGT [66]		-	-	-	33.9	55.2	73.4
UFM560-refine [86]		-	-	-	<b>31.6</b>	<b>54.1</b>	70.9
<b>Ours (stage 1)</b>		55.5	71.1	82.8	<u>29.5</u>	<u>52.6</u>	<u>71.2</u>
<b>Ours (stage 2)</b>		54.2	69.8	81.8	29.1	52.5	<b>71.3</b>

Table 4. **Visual localization results (2D-2D matching) on the InLoc [58] dataset.** We report the percentage of query images localized within 0.25/0.5/1.0 meters and 2/5/10 degrees of the ground-truth pose (higher is better). **Bold** and underline highlights best and second best results.

Method	DUC1	DUC2
SP + SG [12, 52]	49.0 / 68.7 / 80.8	53.4 / 77.1 / 82.4
LoFTR [55]	47.5 / 72.2 / 84.8	54.2 / 74.8 / 85.5
PATS [44]	55.6 / 71.2 / 81.0	58.8 / 80.9 / 85.5
DKM [18]	51.5 / 75.3 / 86.9	63.4 / 82.4 / 87.8
CasMTR [5]	53.5 / 76.8 / 85.4	51.9 / 70.2 / 83.2
RoMa [19]	<b>60.1 / 79.3 / 89.9</b>	<u>66.4 / 83.2 / 87.8</u>
MASt3R [31]	<u>56.1 / 79.3 / 90.9</u>	<b>71.0 / 87.0 / 91.6</b>
<b>Ours (stage 2)</b>	<u>56.1 / 79.3 / 89.4</u>	61.1 / 80.2 / 84.0

ing decoder benefits from stacking multiple dual-stream Transformer layers, *which validates our core contribution*. The performance plateaus after 3 decoder layers likely because of the limited capacity in the small-scale model. Regarding the feature upsampling ratio, we can see that larger resolutions are generally helpful until  $8\times$  upsampling. To balance the accuracy and efficiency, we use  $4\times$  upsampling.

### 4.3. Comparisons with Other Methods

In this section, we compare our large-scale unified model against other task-specific methods.

**2D-2D Benchmarks.** We compare our model with recent 2D-2D SOTA approaches [19, 31, 66, 86] on two-view geometry benchmarks MegaDepth-1500 [36] and ScanNet-1500 [11] in Table 3. We use valid keypoints detected by RoMa [19] to query our model. Our unified model shows strong generalization on ScanNet-1500 achieving an AUC@20° score of over 71 among methods which are not supervised on the ScanNet dataset itself. Our method out-

Table 5. **Image-to-Point (2D-3D) matching comparison on 7Scenes and RGB-D Scenes V2.** We report Inlier Ratio (IR), Feature Matching Ratio (FMR) and the Registration Recall (RR). **Bold** and underline highlights best and second best results.

Methods	7Scenes			RGB-D Scenes V2		
	IR ↑	FMR ↑	RR ↑	IR ↑	FMR ↑	RR ↑
FCGF-2D3D [9]	22.8	78.8	61.4	8.1	27.1	30.4
Predator-2D3D [25]	23.4	77.5	48.5	15.7	59.6	38.4
P2-Net [63]	31.7	79.0	65.7	12.2	65.9	30.2
2D3D-MATR [33]	50.1	92.1	75.8	32.4	90.8	56.4
B2-3Dnet [8]	50.9	<b>93.1</b>	77.7	<u>35.1</u>	<u>94.4</u>	63.4
FreeReg [64]	-	-	-	30.9	82.0	57.3
Diff-Reg [71]	<u>59.1</u>	92.5	<u>83.8</u>	-	-	<u>87.4</u>
<b>Ours (stage 2)</b>	<b>82.4</b>	<u>93.0</u>	<b>91.0</b>	<b>83.6</b>	<b>97.0</b>	<b>92.5</b>

performs MASt3R [31] using the same coarse-to-fine inference pipeline on MegaDepth-1500 and it is the third best model compared to other task-specific SOTA 2D-2D models. It is important to note that DKM [18] and RoMa [19] achieve better results on the MegaDepth benchmark by warping high-resolution image features for improved sub-pixel accuracy. However, this approach is inapplicable to 2D-3D correspondence, as warping from a 2D grid to 3D is undefined. For the InLoc [58] benchmark, we query our model with keypoints sampled from an uniformly spaced grid. Our model achieves competitive results to SOTA models as reported in Table 4.

**2D-3D Benchmarks.** For 2D-3D, we compare our unified model with SOTA on the 7Scenes [21] and RGB-D Scenes V2 [30] test split containing 2304 and 497 image-to-point pairs, respectively. We use the ground-truth keypoints to query our model. Compared with other *dataset-specific* 2D-3D methods reported in Table 5, which are trained and evaluated separately on each dataset, our unified model achieves the best results, outperforming other methods by 8% on *registration recall* (RR) on the 7Scenes dataset.

**3D-3D Benchmarks.** We report 3D-3D registration results on 3DMatch [83], 3DLoMatch [83] and ModelNet [73] test split containing 1623, 1781, and 1266 point-to-point pairs, respectively. We use ground truth keypoints from 3DMatch for correspondence evaluation, and on ModelNet we query the entire source point cloud and apply a cycle consistency check with matching threshold  $\tau_{\text{cycle}} = 0.02$  to filter out the set of invalid correspondences. Similar to 2D-3D, our unified model shows a 10% improvement on *registration recall* (RR) in the challenging low overlap 3DLoMatch benchmark compared the best *dataset-specific* model in Table 6.

It is worth noting that using ground-truth keypoints for 2D-3D and 3D-3D matching does not necessarily put our model in a more advantageous position than others. On the one hand, existing work [25, 33, 48, 70] uses ground truth transformation to align their predictions in order to evaluate their matched pairs whereas our model directly re-

Table 6. **Point-to-Point (3D-3D) matching comparison on 3DMatch, 3DLoMatch, and ModelNet.** We report Inlier Ratio (IR), Feature Matching Ratio (FMR), Registration Recall (RR), Relative Rotation Error (RRE), Relative Translation Error (RTE) and Chamfer Distance (CD). **Bold** and underline highlights best and second best results.

Methods	3DMatch			3DLoMatch				ModelNet		
	IR $\uparrow$	FMR $\uparrow$	RR $\uparrow$	IR $\uparrow$	FMR $\uparrow$	RR $\uparrow$	RRE[ $^\circ$ ] $\downarrow$	RTE[m] $\downarrow$	RRE $\downarrow$	RTE $\downarrow$
FCGF [9]	56.8	97.4	85.1	21.4	76.6	40.1	3.147	0.100	-	-
D3Feat [1]	39.0	95.6	81.6	13.2	67.3	37.2	3.361	0.103	-	-
Cofinet [79]	49.8	98.1	89.3	24.4	83.1	67.5	-	-	-	-
Predator [25]	58.8	96.6	89.0	26.7	78.6	59.8	3.048	0.093	1.739	0.019
RegTR [78]	-	-	92.0	-	-	64.8	2.827	<u>0.077</u>	1.473	0.014
GeoT [48]	70.3	97.7	91.5	43.3	88.1	74.0	<u>2.547</u>	<b>0.074</b>	1.568	0.018
RoITr [80]	82.6	98.0	91.9	54.3	89.6	74.8	-	-	-	-
PEAL-3D [82]	73.3	<b>99.0</b>	94.6	49.0	87.6	79.0	2.788	0.087	-	-
Diff-Reg [71]	30.9	96.3	95.0	9.6	69.6	73.8	-	-	-	-
<b>Ours (stage 1)</b>	<u>95.1</u>	<u>98.5</u>	<u>97.4</u>	<b>77.3</b>	<b>93.2</b>	<b>86.7</b>	3.193	0.168	<b>1.189</b>	<b>0.011</b>
<b>Ours (stage 2)</b>	<b>95.2</b>	98.4	<b>97.5</b>	<u>75.0</u>	<u>90.8</u>	<u>83.2</u>	<b>2.393</b>	0.152	<u>1.324</u>	<u>0.012</u>

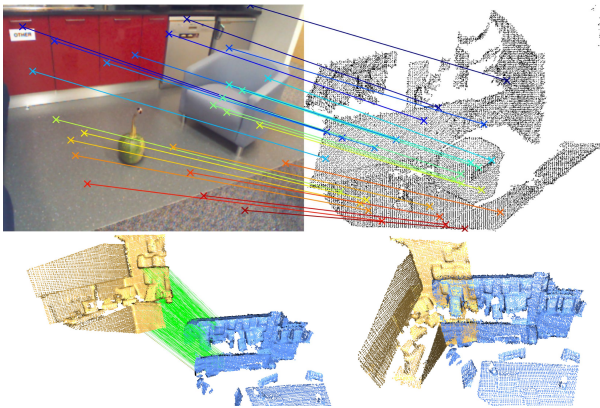


Figure 6. **Visual results of 2D-3D matching on 7Scenes (top) and 3D-3D matching on 3DLoMatch (bottom).** On the bottom left are point cloud pairs with predicted correspondences, and on the bottom right are registered point clouds using transformations estimated via RANSAC. Zoom in for details.

gresses the estimated correspondences in the target coordinate space. On the other hand, we show that on ModelNet, using only cycle consistency check without relying on ground-truth keypoints leads to lower errors than other methods.

#### 4.4. On the Joint Training of Different Tasks

An important question for unified models is whether joint training across tasks provides synergistic benefits. We compare our stage 1 and stage 2 models on 2D-2D and 3D-3D tasks in Tables 3 and 6. Results show that joint training

Table 7. Single task vs. joint training performances.

Methods	MegaDepth (2D-2D)	7Scenes (2D-3D)	3DLoMatch (3D-3D)
	AUC@5 $^\circ$ $\uparrow$	RR $\uparrow$	RR $\uparrow$
Ours (single task)	<b>56.5</b>	67.7	81.8
Ours (joint training)	54.2	<b>91.0</b>	<b>83.2</b>



Figure 5. **Visual results of 2D-2D matching on MegaDepth.** Green/red lines indicate inlier/outlier correspondences. Zoom in for details.

on all three tasks (stage 2) does not consistently outperform stage 1 (2D-2D and 3D-3D only). To investigate this, we analyzed gradient conflicts using the GCD metric [6]. While most parameters show aligned-to-orthogonal gradients (indicating minimal interference), normalization layers exhibit substantial conflicts. This suggests that normalization layers struggle to accommodate the different statistical properties of 2D image and 3D point features when computing shared statistics across modalities.

Despite these conflicts, our model shows significant improvement on 7Scenes (2D-3D) with joint training, as shown in Table 7, indicating mutual benefits from the data-rich 2D-2D domain and demonstrating that the unified architecture provides a reasonable trade-off. Future work could explore better normalization strategies or improved cross-modality alignment designs.

## 5. Conclusion

We presented UniCorrn, the first correspondence model with shared weights that unifies geometric matching across 2D-2D, 2D-3D, and 3D-3D modalities. Our dual-stream Transformer decoder, which decouples appearance and positional features, enables robust correspondence learning across heterogeneous representations. Trained jointly on diverse data, UniCorrn achieves competitive 2D-2D performance and sets new state-of-the-art on 2D-3D and 3D-3D matching tasks. This work demonstrates the feasibility and benefits of unified correspondence modeling. We believe this work represents an important step toward general-purpose correspondence models and hope it inspires further research in unified geometric understanding across different modalities.

## 6. Acknowledgment

This project was partially supported by the National Science Foundation under Award IIS-2310254.

## References

- [1] Xuyang Bai, Zixin Luo, Lei Zhou, Hongbo Fu, Long Quan, and Chiew-Lan Tai. D3feat: Joint learning of dense detection and description of 3d local features. In *Proceedings of the IEEE/CVF conference on computer vision and pattern recognition*, pages 6359–6367, 2020. 2, 3, 8
- [2] Gilad Baruch, Zhuoyuan Chen, Afshin Dehghan, Yuri Feigin, Peter Fu, Thomas Gebauer, Daniel Kurz, Tal Dimry, Brandon Joffe, Arik Schwartz, and Elad Shulman. ARK-itscenes: A diverse real-world dataset for 3d indoor scene understanding using mobile RGB-d data. In *Thirty-fifth Conference on Neural Information Processing Systems Datasets and Benchmarks Track (Round 1)*, 2021. 5, 7
- [3] Liefeng Bo, Xiaofeng Ren, and Dieter Fox. Kernel descriptors for visual recognition. *Advances in neural information processing systems*, 23, 2010. 5
- [4] Anthony Burghoffer, Jérémy Seyssaud, and Baptiste Magnier. Ov<sup>2</sup>slam on euroc MAV datasets: a study of corner detector performance. In *IST*, pages 1–5. IEEE, 2023. 1
- [5] Chenjie Cao and Yanwei Fu. Improving transformer-based image matching by cascaded capturing spatially informative keypoints. In *Proceedings of the IEEE/CVF international conference on computer vision*, 2023. 7
- [6] Heyan Chai, Zeyu Liu, Yongxin Tong, Ziyi Yao, Binxing Fang, and Qing Liao. Towards task-conflicts momentum-calibrated approach for multi-task learning. In *2024 IEEE 40th International Conference on Data Engineering (ICDE)*, pages 939–952. IEEE, 2024. 8
- [7] Hongkai Chen, Zixin Luo, Lei Zhou, Yurun Tian, Mingmin Zhen, Tian Fang, David McKinnon, Yanghai Tsing, and Long Quan. Aspanformer: Detector-free image matching with adaptive span transformer. In *ECCV (32)*, pages 20–36. Springer, 2022. 2, 6, 7
- [8] Zhixin Cheng, Jiacheng Deng, Xinjun Li, Baoqun Yin, and Tianzhu Zhang. Bridge 2d-3d: Uncertainty-aware hierarchical registration network with domain alignment. In *AAAI*, pages 2491–2499. AAAI Press, 2025. 1, 3, 7, 8
- [9] Christopher Choy, Jaesik Park, and Vladlen Koltun. Fully convolutional geometric features. In *ICCV*, pages 8958–8966, 2019. 7, 8
- [10] Christopher B. Choy, JunYoung Gwak, Silvio Savarese, and Manmohan Krishna Chandraker. Universal correspondence network. In *NeurIPS*, 2016. 1, 2, 3
- [11] Angela Dai, Angel X. Chang, Manolis Savva, Maciej Halber, Thomas Funkhouser, and Matthias Nießner. Scannet: Richly-annotated 3d reconstructions of indoor scenes. In *Proc. Computer Vision and Pattern Recognition (CVPR)*, IEEE, 2017. 7
- [12] Daniel DeTone, Tomasz Malisiewicz, and Andrew Rabinovich. Superpoint: Self-supervised interest point detection and description. In *2018 IEEE Conference on Computer Vision and Pattern Recognition Workshops, CVPR Workshops 2018, Salt Lake City, UT, USA, June 18-22, 2018*, pages 224–236. Computer Vision Foundation / IEEE Computer Society, 2018. 2, 3, 7
- [13] Carl Doersch, Ankush Gupta, Larisa Markeeva, Adrià Recasens, Lucas Smaira, Yusuf Aytar, João Carreira, Andrew Zisserman, and Yi Yang. Tap-vid: A benchmark for tracking any point in a video. In *NeurIPS*, 2022. 2
- [14] Carl Doersch, Yi Yang, Mel Vecerík, Dilara Gokay, Ankush Gupta, Yusuf Aytar, João Carreira, and Andrew Zisserman. TAPIR: tracking any point with per-frame initialization and temporal refinement. In *ICCV*, pages 10027–10038. IEEE, 2023. 2
- [15] Siyan Dong, Shuzhe Wang, Shaohui Liu, Lulu Cai, Qingnan Fan, Juho Kannala, and Yanchao Yang. Reloc3r: Large-scale training of relative camera pose regression for generalizable, fast, and accurate visual localization. *CoRR*, abs/2412.08376, 2024. 1
- [16] Alexey Dosovitskiy, Philipp Fischer, Eddy Ilg, Philip Häusser, Caner Hazirbas, Vladimir Golkov, Patrick van der Smagt, Daniel Cremers, and Thomas Brox. FlowNet: Learning optical flow with convolutional networks. In *ICCV*, pages 2758–2766. IEEE Computer Society, 2015. 4
- [17] Alexey Dosovitskiy, Lucas Beyer, Alexander Kolesnikov, Dirk Weissenborn, Xiaohua Zhai, Thomas Unterthiner, Mostafa Dehghani, Matthias Minderer, Georg Heigold, Sylvain Gelly, Jakob Uszkoreit, and Neil Houlsby. An image is worth 16x16 words: Transformers for image recognition at scale. In *ICLR*. OpenReview.net, 2021. 3, 2, 7
- [18] Johan Edstedt, Ioannis Athanasiadis, Mårten Wadenbäck, and Michael Felsberg. DKM: dense kernelized feature matching for geometry estimation. In *CVPR*, pages 17765–17775. IEEE, 2023. 1, 2, 7
- [19] Johan Edstedt, Qiyu Sun, Georg Bökman, Mårten Wadenbäck, and Michael Felsberg. Roma: Robust dense feature matching. In *CVPR*, pages 19790–19800. IEEE, 2024. 2, 3, 7, 6
- [20] Mengdan Feng, Sixing Hu, Marcelo H. Ang, and Gim Hee Lee. 2d3d-matchnet: Learning to match keypoints across 2d image and 3d point cloud. In *ICRA*, pages 4790–4796. IEEE, 2019. 2
- [21] Ben Glocker, Shahram Izadi, Jamie Shotton, and Antonio Criminisi. Real-time rgb-d camera relocalization. In *2013 IEEE International Symposium on Mixed and Augmented Reality (ISMAR)*, pages 173–179, 2013. 2, 5, 7, 4, 8
- [22] Aniket Gupta, Yiming Xie, Hanumant Singh, and Huaizu Jiang. Direct superpoints matching for fast and robust point cloud registration. *CoRR*, abs/2307.01362, 2023. 1, 3, 4
- [23] Xingyi He, Hao Yu, Sida Peng, Dongli Tan, Zehong Shen, Hujun Bao, and Xiaowei Zhou. Matchanything: Universal cross-modality image matching with large-scale pre-training. In *Arxiv*, 2025. 1, 2, 3
- [24] Jonathan Ho, Ajay Jain, and Pieter Abbeel. Denoising diffusion probabilistic models. *CoRR*, abs/2006.11239, 2020. 3
- [25] Shengyu Huang, Zan Gojcic, Mikhail Usvyatsov, Andreas Wieser, and Konrad Schindler. Predator: Registration of 3d point clouds with low overlap. In *Proceedings of*

- the *IEEE/CVF Conference on computer vision and pattern recognition*, pages 4267–4276, 2021. 1, 3, 6, 7, 8
- [26] Wei Jiang, Eduard Trulls, Jan Hosang, Andrea Tagliasacchi, and Kwang Moo Yi. COTR: correspondence transformer for matching across images. In *ICCV*, pages 6187–6197. IEEE, 2021. 2, 4, 6
- [27] Shuhao Kang, Youqi Liao, Jianping Li, Fuxun Liang, Yuhao Li, Xianghong Zou, Fangning Li, Xieyuanli Chen, Zhen Dong, and Bisheng Yang. Cofii2p: Coarse-to-fine correspondences-based image to point cloud registration. *IEEE Robotics Autom. Lett.*, 9(11):10264–10271, 2024. 3
- [28] Nikita Karaev, Iurii Makarov, Jianyuan Wang, Natalia Neverova, Andrea Vedaldi, and Christian Rupprecht. Co-tracker3: Simpler and better point tracking by pseudo-labelling real videos. *CoRR*, abs/2410.11831, 2024. 2
- [29] Alexander Kirillov, Eric Mintun, Nikhila Ravi, Hanzi Mao, Chloé Rolland, Laura Gustafson, Tete Xiao, Spencer Whitehead, Alexander C. Berg, Wan-Yen Lo, Piotr Dollár, and Ross B. Girshick. Segment anything. In *ICCV*, 2023. 2
- [30] Kevin Lai, Liefeng Bo, and Dieter Fox. Unsupervised feature learning for 3d scene labeling. In *2014 IEEE International Conference on Robotics and Automation (ICRA)*, pages 3050–3057, 2014. 5, 7, 4
- [31] Vincent Leroy, Yohann Cabon, and Jérôme Revaud. Grounding image matching in 3d with mast3r. In *ECCV (72)*, pages 71–91. Springer, 2024. 2, 3, 5, 6, 7
- [32] Jiaxin Li and Gim Hee Lee. Deepi2p: Image-to-point cloud registration via deep classification. In *CVPR*, pages 15960–15969. Computer Vision Foundation / IEEE, 2021. 3
- [33] Minhao Li, Zheng Qin, Zhirui Gao, Renjiao Yi, Chenyang Zhu, Yulan Guo, and Kai Xu. 2d3d-matr: 2d-3d matching transformer for detection-free registration between images and point clouds. In *ICCV*, pages 14082–14092. IEEE, 2023. 1, 3, 4, 6, 7, 2, 8
- [34] Yang Li and Tatsuya Harada. Leopard: Learning partial point cloud matching in rigid and deformable scenes. In *Proceedings of the IEEE/CVF Conference on Computer Vision and Pattern Recognition (CVPR)*, pages 5554–5564, 2022. 3
- [35] Yang Li and Tatsuya Harada. Leopard: Learning partial point cloud matching in rigid and deformable scenes. In *IEEE/CVF Conference on Computer Vision and Pattern Recognition, CVPR 2022, New Orleans, LA, USA, June 18–24, 2022*, pages 5544–5554. IEEE, 2022. 2
- [36] Zhengqi Li and Noah Snavely. Megadepth: Learning single-view depth prediction from internet photos. In *Proceedings of the IEEE conference on computer vision and pattern recognition*, pages 2041–2050, 2018. 5, 7
- [37] Philipp Lindenberger, Paul-Edouard Sarlin, and Marc Pollefeys. Lightglue: Local feature matching at light speed. In *ICCV*, pages 17581–17592. IEEE, 2023. 7
- [38] Ilya Loshchilov and Frank Hutter. Decoupled weight decay regularization. In *7th International Conference on Learning Representations, ICLR 2019, New Orleans, LA, USA, May 6–9, 2019*. OpenReview.net, 2019. 7
- [39] David G. Lowe. Distinctive image features from scale-invariant keypoints. *Int. J. Comput. Vis.*, 60(2):91–110, 2004. 3
- [40] David G Lowe. Distinctive image features from scale-invariant keypoints. *International journal of computer vision*, 60:91–110, 2004. 5
- [41] David G. Lowe. Distinctive image features from scale-invariant keypoints. *Int. J. Comput. Vis.*, 60(2):91–110, 2004. 2
- [42] Nikolaus Mayer, Eddy Ilg, Philip Häusser, Philipp Fischer, Daniel Cremers, Alexey Dosovitskiy, and Thomas Brox. A large dataset to train convolutional networks for disparity, optical flow, and scene flow estimation. In *2016 IEEE Conference on Computer Vision and Pattern Recognition (CVPR)*, pages 4040–4048, 2016. 5, 7
- [43] Eliakim H Moore. On the reciprocal of the general algebraic matrix. *Bulletin of the american mathematical society*, 26: 294–295, 1920. 5
- [44] Junjie Ni, Yijin Li, Zhaoyang Huang, Hongsheng Li, Hujun Bao, Zhaopeng Cui, and Guofeng Zhang. PATS: patch area transportation with subdivision for local feature matching. In *CVPR*, pages 17776–17786. IEEE, 2023. 2, 7
- [45] Maxime Oquab, Timothée Darcet, Théo Moutakanni, Huy V. Vo, Marc Szafraniec, Vasil Khalidov, Pierre Fernandez, Daniel Haziza, Francisco Massa, Alaaeldin El-Nouby, Mido Assran, Nicolas Ballas, Wojciech Galuba, Russell Howes, Po-Yao Huang, Shang-Wen Li, Ishan Misra, Michael Rabbat, Vasu Sharma, Gabriel Synnaeve, Hu Xu, Hervé Jégou, Julien Mairal, Patrick Labatut, Armand Joulin, and Piotr Bojanowski. Dinov2: Learning robust visual features without supervision. *Trans. Mach. Learn. Res.*, 2024, 2024. 2, 3
- [46] Roger Penrose. A generalized inverse for matrices. In *Mathematical proceedings of the Cambridge philosophical society*, pages 406–413. Cambridge University Press, 1955. 5
- [47] Quang-Hieu Pham, Mikaela Angelina Uy, Binh-Son Hua, Duc Thanh Nguyen, Gemma Roig, and Sai-Kit Yeung. LCD: learned cross-domain descriptors for 2d-3d matching. In *AAAI*, pages 11856–11864. AAAI Press, 2020. 2
- [48] Zheng Qin, Hao Yu, Changjian Wang, Yulan Guo, Yuxing Peng, and Kai Xu. Geometric transformer for fast and robust point cloud registration. In *CVPR*, pages 11133–11142. IEEE, 2022. 1, 3, 7, 8
- [49] Jeremy Reizenstein, Roman Shapovalov, Philipp Henzler, Luca Sbordone, Patrick Labatut, and David Novotný. Common objects in 3d: Large-scale learning and evaluation of real-life 3d category reconstruction. *CoRR*, abs/2109.00512, 2021. 5, 7
- [50] Jérôme Revaud, César Roberto de Souza, Martin Humenberger, and Philippe Weinzaepfel. R2D2: reliable and repeatable detector and descriptor. In *NeurIPS*, pages 12405–12415, 2019. 2
- [51] Robin Rombach, Andreas Blattmann, Dominik Lorenz, Patrick Esser, and Björn Ommer. High-resolution image synthesis with latent diffusion models. *CoRR*, abs/2112.10752, 2021. 3
- [52] Paul-Edouard Sarlin, Daniel DeTone, Tomasz Malisiewicz, and Andrew Rabinovich. Superglue: Learning feature matching with graph neural networks. In *CVPR*, pages 4937–4946. Computer Vision Foundation / IEEE, 2020. 2, 6, 7
- [53] Wenzhe Shi, Jose Caballero, Ferenc Huszar, Johannes Totz, Andrew P. Aitken, Rob Bishop, Daniel Rueckert, and Zehan

- Wang. Real-time single image and video super-resolution using an efficient sub-pixel convolutional neural network. In *2016 IEEE Conference on Computer Vision and Pattern Recognition, CVPR 2016, Las Vegas, NV, USA, June 27-30, 2016*, pages 1874–1883. IEEE Computer Society, 2016. 4, 6
- [54] Jianlin Su, Murtadha H. M. Ahmed, Yu Lu, Shengfeng Pan, Wen Bo, and Yunfeng Liu. Roformer: Enhanced transformer with rotary position embedding. *Neurocomputing*, 568:127063, 2024. 3, 4
- [55] Jiaming Sun, Zehong Shen, Yuang Wang, Hujun Bao, and Xiaowei Zhou. Loftr: Detector-free local feature matching with transformers. In *CVPR*, pages 8922–8931. Computer Vision Foundation / IEEE, 2021. 1, 2, 3, 4, 6, 7
- [56] Pei Sun, Henrik Kretzschmar, Xerxes Dotiwalla, Aurelien Chouard, Vijaysai Patnaik, Paul Tsui, James Guo, Yin Zhou, Yuning Chai, Benjamin Caine, Vijay Vasudevan, Wei Han, Jiquan Ngiam, Hang Zhao, Aleksei Timofeev, Scott Ettinger, Maxim Krivokon, Amy Gao, Aditya Joshi, Yu Zhang, Jonathon Shlens, Zhifeng Chen, and Dragomir Anguelov. Scalability in perception for autonomous driving: Waymo open dataset. In *2020 IEEE/CVF Conference on Computer Vision and Pattern Recognition, CVPR 2020, Seattle, WA, USA, June 13-19, 2020*, pages 2443–2451. Computer Vision Foundation / IEEE, 2020. 5, 7
- [57] Yifan Sun, Changmao Cheng, Yuhan Zhang, Chi Zhang, Liang Zheng, Zhongdao Wang, and Yichen Wei. Circle loss: A unified perspective of pair similarity optimization. *CoRR*, abs/2002.10857, 2020. 3
- [58] Hajime Taira, Masatoshi Okutomi, Torsten Sattler, Mircea Cimpoi, Marc Pollefeys, Josef Sivic, Tomás Pajdla, and Akihiko Torii. Inloc: Indoor visual localization with dense matching and view synthesis. In *2018 IEEE Conference on Computer Vision and Pattern Recognition, CVPR 2018, Salt Lake City, UT, USA, June 18-22, 2018*, pages 7199–7209. Computer Vision Foundation / IEEE Computer Society, 2018. 7, 2, 5, 6
- [59] Prune Truong, Martin Danelljan, and Radu Timofte. Glunet: Global-local universal network for dense flow and correspondences. In *CVPR*, 2020. 1, 2, 3
- [60] Michal J. Tyszkiewicz, Pascal Fua, and Eduard Trulls. DISK: learning local features with policy gradient. In *NeurIPS*, 2020. 2
- [61] Aäron van den Oord, Yazhe Li, and Oriol Vinyals. Representation learning with contrastive predictive coding. *CoRR*, abs/1807.03748, 2018. 5, 1
- [62] Ashish Vaswani, Noam Shazeer, Niki Parmar, Jakob Uszkoreit, Llion Jones, Aidan N Gomez, Łukasz Kaiser, and Illia Polosukhin. Attention is all you need. *Advances in neural information processing systems*, 30, 2017. 2, 3, 1
- [63] Bing Wang, Changhao Chen, Zhaopeng Cui, Jie Qin, Chris Xiaoxuan Lu, Zhengdi Yu, Peijun Zhao, Zhen Dong, Fan Zhu, Niki Trigoni, et al. P2-net: Joint description and detection of local features for pixel and point matching. In *ICCV*, pages 16004–16013, 2021. 3, 7, 8
- [64] Haiping Wang, Yuan Liu, Bing Wang, Yujing Sun, Zhen Dong, Wenping Wang, and Bisheng Yang. Freereg: Image-to-point cloud registration leveraging pretrained diffusion models and monocular depth estimators. In *ICLR. Open-Review.net*, 2024. 3, 7
- [65] Jianyuan Wang, Nikita Karaev, Christian Rupprecht, and David Novotný. Vggsfm: Visual geometry grounded deep structure from motion. In *CVPR*, pages 21686–21697. IEEE, 2024. 1
- [66] Jianyuan Wang, Minghao Chen, Nikita Karaev, Andrea Vedaldi, Christian Rupprecht, and David Novotny. Vggt: Visual geometry grounded transformer. *arXiv preprint arXiv:2503.11651*, 2025. 2, 3, 7
- [67] Shuzhe Wang, Vincent Leroy, Yohann Cabon, Boris Chidlovskii, and Jérôme Revaud. Dust3r: Geometric 3d vision made easy. In *CVPR*, pages 20697–20709. IEEE, 2024. 2, 3
- [68] Yifan Wang, Xingyi He, Sida Peng, Dongli Tan, and Xiaowei Zhou. Efficient loftr: Semi-dense local feature matching with sparse-like speed. In *CVPR*, pages 21666–21675. IEEE, 2024. 2, 3, 7
- [69] Philippe Weinzaepfel, Thomas Lucas, Vincent Leroy, Yohann Cabon, Vaibhav Arora, Romain Brégier, Gabriela Csurka, Leonid Antsfeld, Boris Chidlovskii, and Jérôme Revaud. Croco v2: Improved cross-view completion pre-training for stereo matching and optical flow. In *ICCV*, pages 17923–17934. IEEE, 2023. 2, 3, 6, 7
- [70] Qianliang Wu, Haobo Jiang, Lei Luo, Jun Li, Yaqing Ding, Jin Xie, and Jian Yang. Diff-reg: Diffusion model in doubly stochastic matrix space for registration problem. In *ECCV (65)*, pages 160–178. Springer, 2024. 3, 7
- [71] Qianliang Wu, Haobo Jiang, Yaqing Ding, Lei Luo, Jin Xie, and Jian Yang. Diff-reg v2: Diffusion-based matching matrix estimation for image matching and 3d registration. *CoRR*, abs/2503.04127, 2025. 7, 8, 2
- [72] Xiaoyang Wu, Li Jiang, Peng-Shuai Wang, Zhijian Liu, Xihui Liu, Yu Qiao, Wanli Ouyang, Tong He, and Hengshuang Zhao. Point transformer V3: simpler, faster, stronger. In *CVPR*, pages 4840–4851. IEEE, 2024. 3, 4, 2, 7
- [73] Zhirong Wu, Shuran Song, Aditya Khosla, Fisher Yu, Linguang Zhang, Xiaoou Tang, and Jianxiong Xiao. 3d shapenets: A deep representation for volumetric shapes. In *2015 IEEE Conference on Computer Vision and Pattern Recognition (CVPR)*, pages 1912–1920, 2015. 5, 6, 7
- [74] Taihong Xiao, Jinwei Yuan, Deqing Sun, Qifei Wang, Xinyu Zhang, Kehan Xu, and Ming-Hsuan Yang. Learnable cost volume using the cayley representation. In *ECCV*, 2020. 4, 1
- [75] Fei Xue, Sven Elfle, Laura Leal-Taixé, and Qunjie Zhou. Matcha: towards matching anything. In *CVPR*, 2025. 1, 2, 3
- [76] Yao Yao, Zixin Luo, Shiwei Li, Jingyang Zhang, Yufan Ren, Lei Zhou, Tian Fang, and Long Quan. Blendedmvs: A large-scale dataset for generalized multi-view stereo networks. *CoRR*, abs/1911.10127, 2019. 5, 7
- [77] Chandan Yeshwanth, Yueh-Cheng Liu, Matthias Nießner, and Angela Dai. Scannet++: A high-fidelity dataset of 3d indoor scenes. In *Proceedings of the International Conference on Computer Vision (ICCV)*, 2023. 5, 1, 7
- [78] Zi Jian Yew and Gim Hee Lee. Regtr: End-to-end point cloud correspondences with transformers. In *Proceedings of*

- the *IEEE/CVF conference on computer vision and pattern recognition*, pages 6677–6686, 2022. 3, 6, 8
- [79] Hao Yu, Fu Li, Mahdi Saleh, Benjamin Busam, and Slobodan Ilic. Cofinet: Reliable coarse-to-fine correspondences for robust pointcloud registration. *Advances in Neural Information Processing Systems*, 34:23872–23884, 2021. 8
- [80] Hao Yu, Zheng Qin, Ji Hou, Mahdi Saleh, Dongsheng Li, Benjamin Busam, and Slobodan Ilic. Rotation-invariant transformer for point cloud matching. In *Proceedings of the IEEE/CVF conference on computer vision and pattern recognition*, pages 5384–5393, 2023. 3, 8
- [81] Jiahuan Yu, Jiahao Chang, Jianfeng He, Tianzhu Zhang, Jiyang Yu, and Feng Wu. Adaptive spot-guided transformer for consistent local feature matching. In *Proceedings of the IEEE/CVF Conference on Computer Vision and Pattern Recognition*, pages 21898–21908, 2023. 2
- [82] Junle Yu, Luwei Ren, Yu Zhang, Wenhui Zhou, Lili Lin, and Guojun Dai. Peal: Prior-embedded explicit attention learning for low-overlap point cloud registration. In *Proceedings of the IEEE/CVF Conference on Computer Vision and Pattern Recognition*, pages 17702–17711, 2023. 3, 8
- [83] Andy Zeng, Shuran Song, Matthias Nießner, Matthew Fisher, Jianxiong Xiao, and Thomas Funkhouser. 3dmatch: Learning local geometric descriptors from rgb-d reconstructions. In *CVPR, 2017*. 2, 3, 5, 6, 7
- [84] Songyan Zhang, Xinyu Sun, Hao Chen, Bo Li, and Chunhua Shen. RGM: A robust generalist matching model. *CoRR*, abs/2310.11755, 2023. 1, 2, 3
- [85] Yushan Zhang, Johan Edstedt, Bastian Wandt, Per-Erik Forssén, Maria Magnusson, and Michael Felsberg. Gmsf: Global matching scene flow. *Advances in Neural Information Processing Systems*, 36:64415–64427, 2023. 6
- [86] Yuchen Zhang, Nikhil Keetha, Chenwei Lyu, Bhuvan Jhamb, Yutian Chen, Yuheng Qiu, Jay Karhade, Shreyas Jha, Yaoyu Hu, Deva Ramanan, Sebastian Scherer, and Wenshan Wang. Ufm: A simple path towards unified dense correspondence with flow. In *arXiv*, 2025. 1, 2, 3, 4, 6, 7
- [87] Xiaoming Zhao, Xingming Wu, Weihai Chen, Peter C. Y. Chen, Qingsong Xu, and Zhengguo Li. ALIKED: A lighter keypoint and descriptor extraction network via deformable transformation. *IEEE Trans. Instrum. Meas.*, 72:1–16, 2023. 3

# UniCorrn: Unified Correspondence Transformer Across 2D and 3D

## Supplementary Material

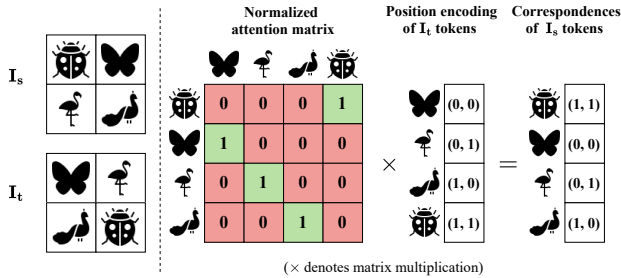


Figure 7. **Illustration of estimating correspondence with attention.** Here each animal symbol denotes a pixel (so both  $I_s$  and  $I_t$  have  $2 \times 2$  pixels.).

### A. Attention as a Learnable Matching Cost

In figure 7, we show an illustration of using attention to estimate correspondences with a toy example. Let’s consider two input images  $I_s$  and  $I_t$ . The attention map  $A$  between them is computed as the softmax-normalized dot product of the flattened inputs. The attention map is row-normalized and one-hot in each row in an ideal case, where the position of 1 corresponds to the correct matching pixel. If we set the vector  $V$  in Transformer to the absolute positional encoding of every pixel in  $I_t$ , as shown in Fig. 7, the output  $AV$  contains the positional encoding of the correct corresponding pixels in  $I_t$  for every pixel in  $I_s$ .

The attention matrix is similar to the normalized version of the learnable cost volume studied in [74]. In practice, while features may not be perfectly discriminative as demonstrated in this example, the methodology of using attention matrix as a matching cost function still applies.

### B. Further Details on Matching Decoder

#### B.1. Gaussian Attention

In the paper, we propose Gaussian attention in replace of vanilla attention [62] within our matching decoder. The attention logits are computed using pairwise squared  $L_2$  distance is formulated as:

$$a_{ij} = -\frac{\|Q_i - K_j\|^2}{D}, \quad (11)$$

where  $Q$  and  $K$  are query and key tokens and  $D$  is the embedding dimension. Furthermore, if we took softmax function into consideration to get the normalized attention scores, the equation becomes:

$$A_{ij} = \frac{\exp(a_{ij})}{\sum_k \exp(a_{ik})}. \quad (12)$$

Here,  $\exp(a)$  fits into the general formulation of the Gaussian kernel.

#### B.2. InfoNCE Loss

We provide further details of computing InfoNCE [61] loss. For a given pair of source and target feature descriptors  $F_s^{desc}$  and  $F_t^{desc}$ , respectively, the InfoNCE loss over the set of ground-truth correspondences  $\mathcal{M} = \{\bar{K}_s(i), \bar{K}_t(i)\}_{i=1}^N$  is given by:

$$\mathcal{L}_c(F_s^{desc}, F_t^{desc}) = -\sum_{i=1}^N \log \frac{d(\bar{K}_s(i), \bar{K}_t(i))}{\sum_{j=1}^N d(\bar{K}_s(j), \bar{K}_t(i))} + \log \frac{d(\bar{K}_s(i), \bar{K}_t(i))}{\sum_{j=1}^N d(\bar{K}_s(i), \bar{K}_t(j))}, \quad (13)$$

$$\text{with } d(\bar{K}_s, \bar{K}_t) = \tau^{-1} \|F_s^{desc}(\bar{K}_s) - F_t^{desc}(\bar{K}_t)\|_2,$$

where  $\tau$  is a temperature hyperparameter. Similarly, we compute the InfoNCE loss for  $\mathcal{L}_c(F_k, F_t^{desc})$ .

#### B.3. Pseudo Point Cloud Data

In Table 8, we show the effectiveness of using pseudo point cloud data for the 2D3D and 3D3D tasks. The pseudo point cloud is generated from dense depth maps, where depth is projected to dense 3D points and sampled with equal strides to resemble the sparse structure of the 3D benchmark datasets. As our approach is data-driven, jointly training with pseudo-point cloud data enables our model to reach SOTA performance.

Table 8. **Effectiveness of pseudo point cloud data** for 2D-3D and 3D-3D task. The pseudo data is sampled from ScanNet++ [77] depth maps.

Pseudo Point Cloud	7Scenes (2D-3D)			3DLoMatch (3D-3D)		
	IR $\uparrow$	FMR $\uparrow$	RR $\uparrow$	IR $\uparrow$	FMR $\uparrow$	RR $\uparrow$
$\times$	12.9	49.5	15.4	51.1	83.2	73.2
$\checkmark$	<b>66.3</b>	<b>88.2</b>	<b>77.8</b>	<b>70.5</b>	<b>90.1</b>	<b>81.8</b>

#### B.4. Auxiliary Supervision

In our training objective, we use intermediate predictions by applying the attention matrix directly over the target coordinates for auxiliary supervision. As shown in Tab. 9, the auxiliary loss produced substantial performance improvement

with a single matching decoder layer and also improved the results while scaling up the number of layers. In Figure. 8 we visualize the attention heatmaps for each decoder layer along with the final predicted coordinates from the model. The heatmaps show a clear difference: without auxiliary supervision, attention patterns are random across layers, while with auxiliary supervision, query tokens consistently attend to their corresponding predicted coordinates. This shows how the dual-stream attention propagates through the matching decoder layers.

Table 9. Effectiveness of auxiliary loss  $\mathcal{L}_{aux}$ .

Number of Layers	$\mathcal{L}_{aux}$	MegaDepth-1500		
		5° ↑	10° ↑	20° ↑
1	✗	28.8	45.3	61.3
1	✓	47.7	64.2	77.2
5	✗	48.5	65.1	77.9
5	✓	50.6	67.1	79.6

### B.5. Additional details on model and training

We train two models with two different capacities. For the small-scale model, we employ 12-layer ViT [17] and PTv3 [72] transformers as image and point cloud backbones, respectively, along with an 8-layer shared Transformer for feature fusion encoder. We ablate various configurations of our matching transformer decoder using this setup in Section 4.2. The large-scale model extends these architectures to 24 and 14 layers for the ViT and PTv3 backbones, and 12 and 8 layers for the feature fusion encoder and matching decoder, respectively. We train the large-scale unified model (600M parameters) in two stages. In the first stage, the model is initialized with the pre-trained weights of CroCo v2 [69] and jointly trained on 2D-2D and 3D-3D tasks with the AdamW optimizer for 40 epochs. This stage uses 384,000 2D-2D pairs and 384,000 of 3D-3D pairs. The second stage is trained on all three tasks for 30 epochs with 60,000 samples per task per epoch. The input images are resized to  $512 \times 384$  for the 2D-2D and 2D-3D tasks. The training runs on  $8 \times H100$  GPUs with stage 1 taking 7 days and stage 2 taking 4 days.

In Table 11, we provide the configurations of each module for our small and large-scale models. Table 12 contains the hyperparameters used for the two stage large-scale training. Finally, Table 13 shows the mixture of 2D-2D, 2D-3D and 3D-3D datasets along with the pseudo data samples used in each stage of large-scale training. We further oversample the 2D-3D and 3D-3D pairs to match the total number of pairs used for the 2D-2D task so that the model can be jointly trained.

## C. Generalization to unseen correspondence tasks

Our model may generalize to other geometry matching tasks, like optical flow without any fine-tuning. On the Sintel final training split, our model achieves an end-point error (EPE) of 5.2 with zero-shot inference (specialist model RAFT reports EPE of 2.71). This is significant because our model was trained exclusively on static, photorealistic imagery, making Sintel’s dynamic motion and stylized rendering strictly out-of-distribution. For other correspondence task, like semantic matching, fine-tuning is required. In fact, unifying both geometric and semantic understanding with a single model by training on all different data is an exciting direction to go.

## D. Inference time and memory usage

The memory footprint of our unified model is  $\sim 2.6G$  which is  $3.5 \times$  less than the combined memory usage of the specialized models. We report the inference time comparisons with specialized models in the table below, measured on an RTX A5000.

Table 10. Inference time in milliseconds(ms) on RTX A5000. Our method uses 5000 keypoint queries. Diff-Reg [71] uses existing models for 2D-3D [33] and 3D-3D [35] feature descriptors.

	ScanNet (2D-2D)	7Scenes (2D-3D)	3DMatch (3D-3D)
Ours	329 ms	390 ms	320 ms
Specialized	203 ms (RoMa)	1140 ms (Diff-Reg)	603 ms (Diff-Reg)

## E. Additional visual results

We show qualitative comparison with state-of-the-art 2D-2D matching methods RoMa [19] and MAST3R [31] in Figure 11. Figure 10 shows the correspondences for different confidence thresholds on two examples from the InLoc [58] benchmark. Additionally, we provide visual results for 2D-3D and 3D-3D in Figure 9 and Figure 12, respectively.

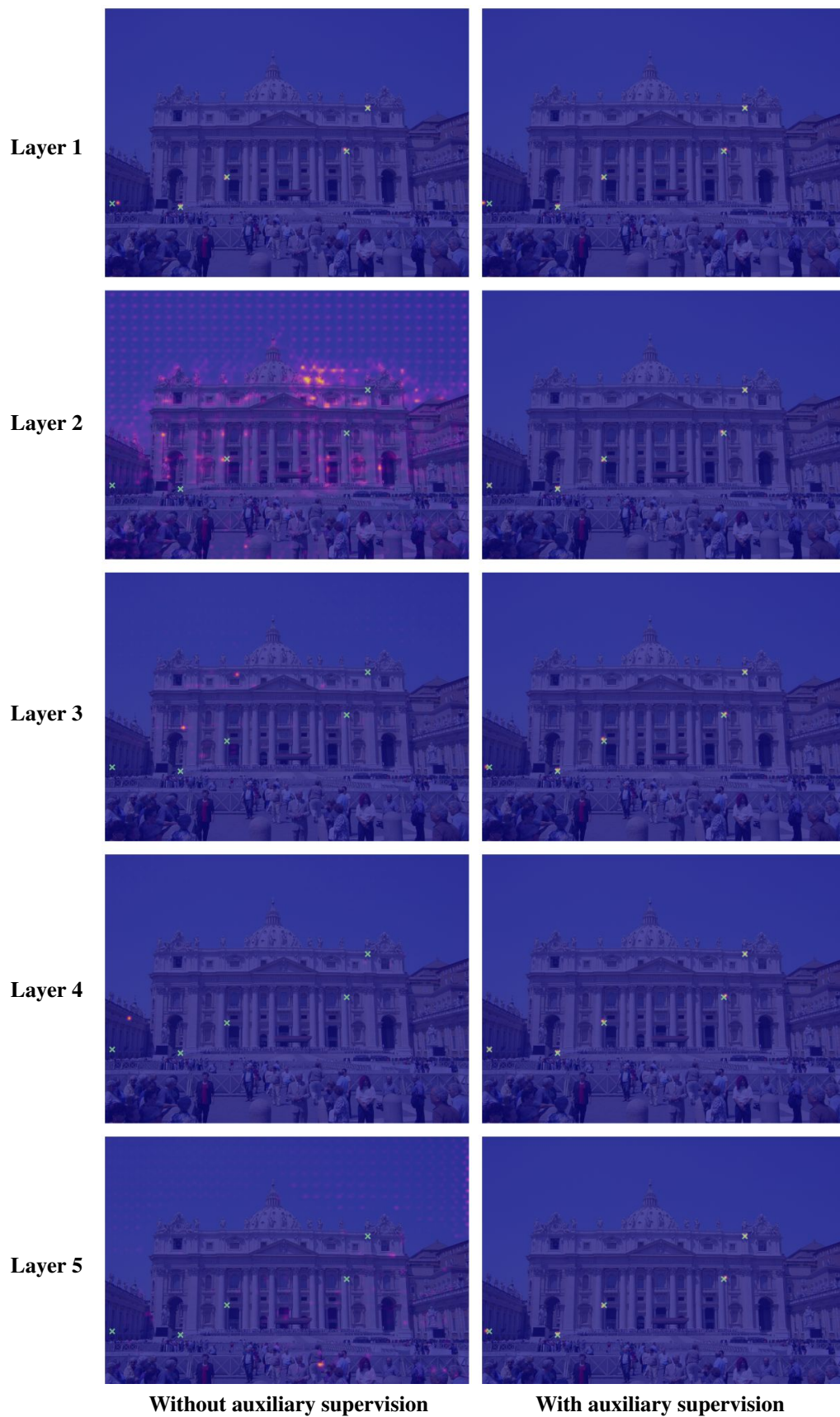


Figure 8. **Per-layer attention heatmap comparison for the effectiveness of auxiliary supervision.** Green markers indicates the model's predicted coordinates. Zoom in for more details.

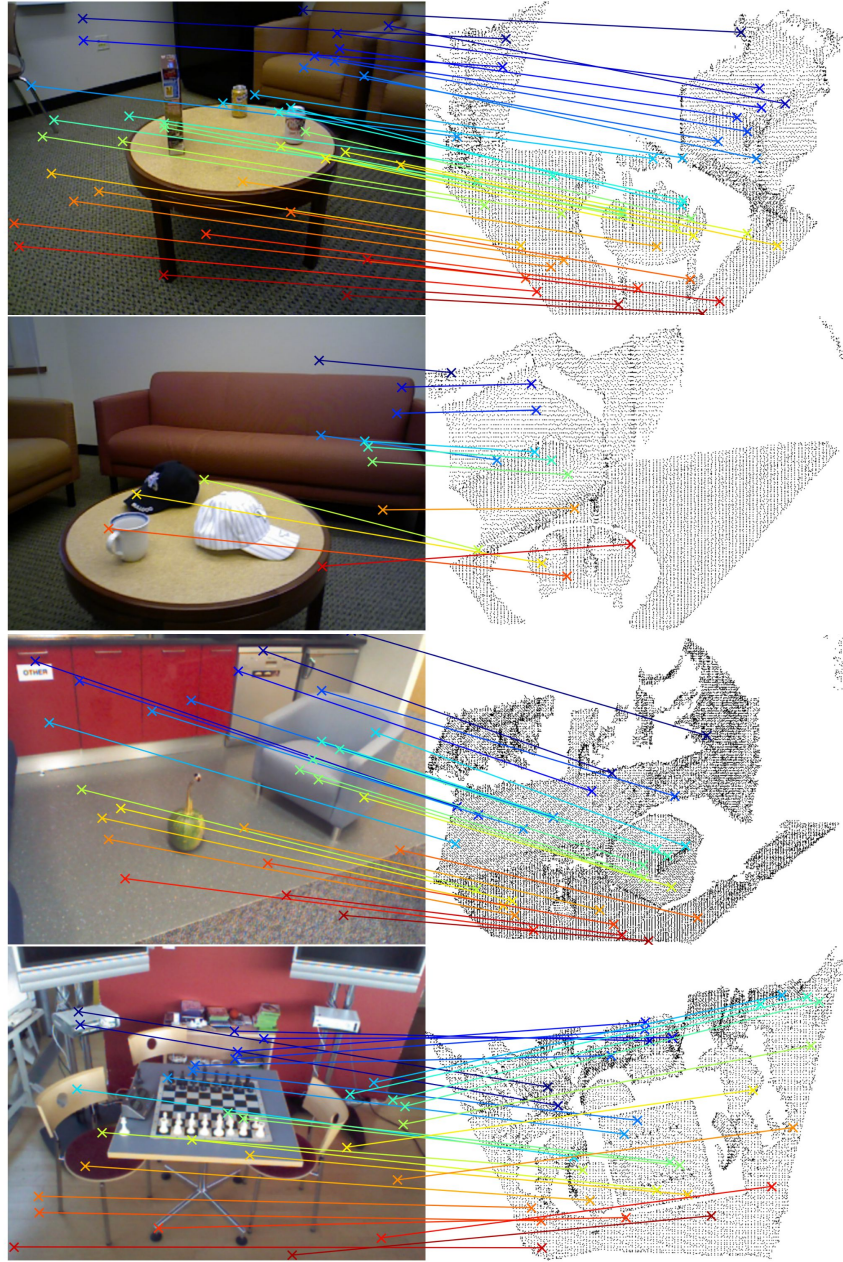
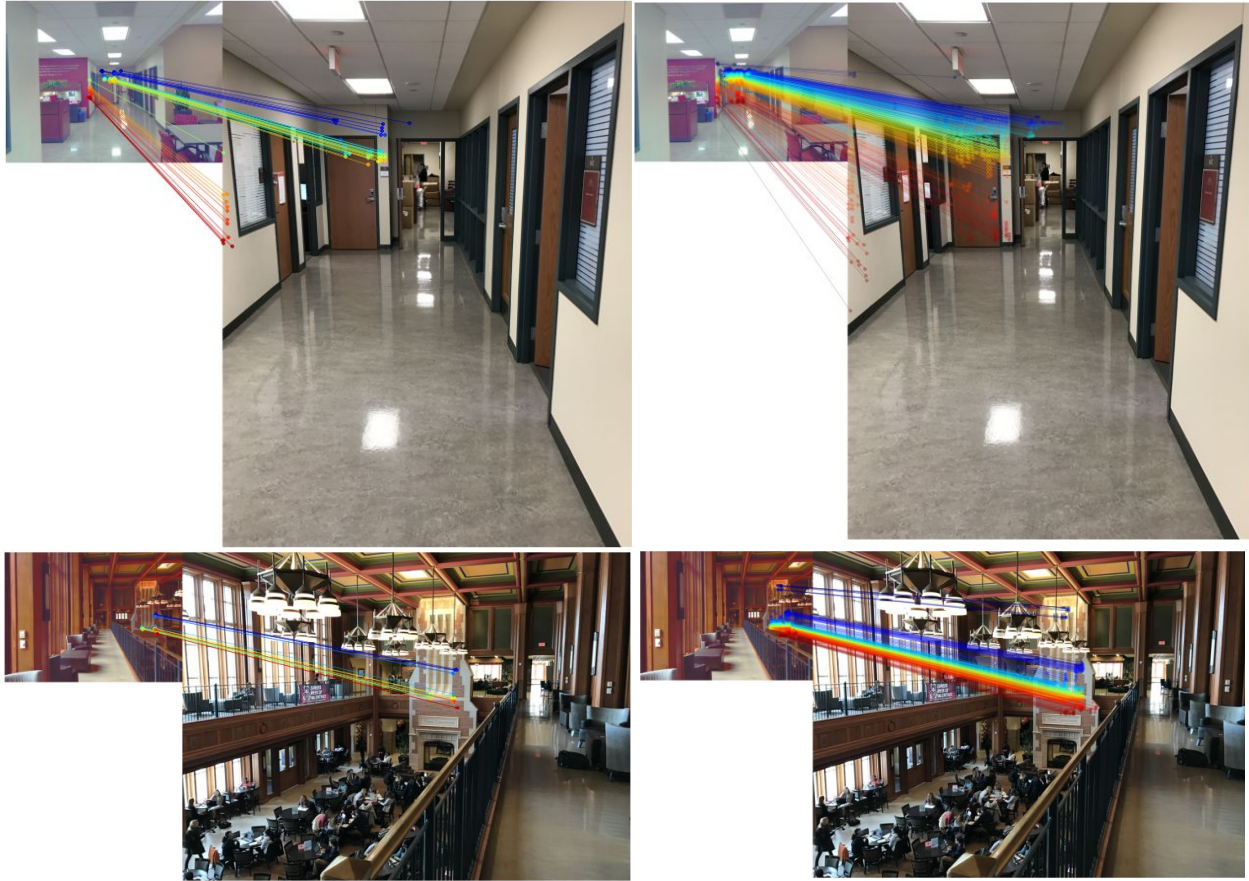


Figure 9. **Visual results of 2D-3D matching on 3DMatch (top) and 3DLoMatch (bottom).** The top two rows are from the RGB-Scenes V2 [30] and the bottom two rows are from 7Scenes [21].



Confidence score > 2.0

Confidence score > 1.5

Figure 10. **Visual results on two examples from the InLoc [58] Benchmark.** We show the correspondences for different confidence thresholds. Zoom in for details.

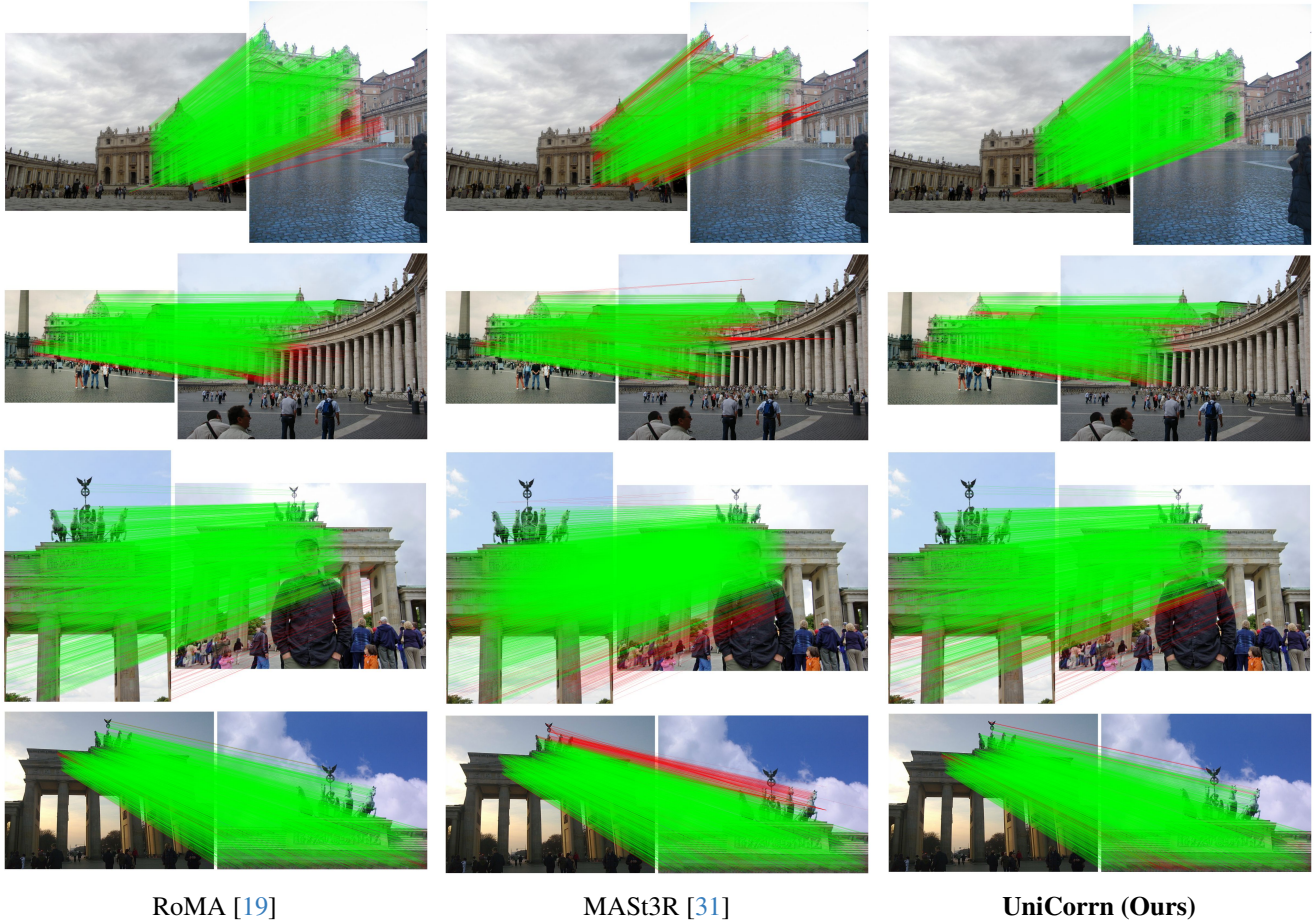


Figure 11. **2D-2D qualitative comparisons on the MegaDepth-1500 benchmark.** Green and red lines indicate accepted and rejected correspondences by the RANSAC essential matrix estimation, respectively. Zoom in for details.

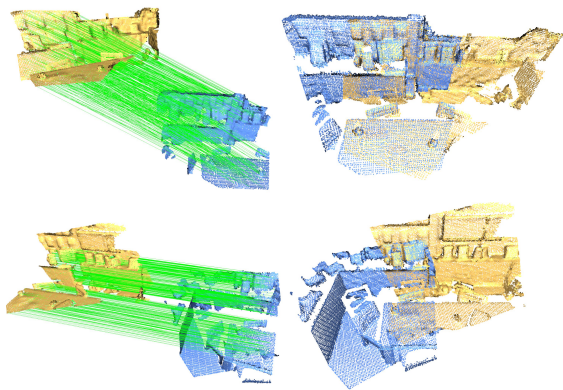


Figure 12. **Visual results of 3D-3D matching on 3DMatch (top) and 3DLoMatch (bottom).** On the left are point cloud pairs with predicted correspondences, and on the right are registered point clouds using transformations estimated via RANSAC.



Figure 13. **Failure case on InLoc [58] benchmark.** The correspondences inside the red ellipse are invalid since the pillar’s face on the first image is not visible on the second image. Hence these correspondences would yield incorrect geometry.

Table 11. **Detailed architecture** of our small-scale and large-scale model.

Module	Type	Attribute	Size
<b>UniCorrn (small-baseline)</b>			
Image backbone	ViT-B [17]	Depth	12
		Heads	12
		Embedding dims	768
Point cloud backbone	PTv3 [72]	Depth	[2, 2, 6, 2]
		Heads	[4, 8, 16, 32]
		Embedding dims	[64, 128, 256, 512]
Feature fusion encoder	Cross-view [69]	Depth	8
		Heads	16
Matching decoder	Dual-stream (ours)	Embedding dims	512
		Depth	8
		Heads	16
		Embedding dims	256
<b>UniCorrn (small-final)</b>			
Image backbone	ViT-B [17]	Depth	12
		Heads	12
		Embedding dims	768
Point cloud backbone	PTv3 [72]	Depth	[2, 6, 4]
		Heads	[2, 8, 32]
		Embedding dims	[32, 128, 512]
Feature fusion encoder	Cross-view [69]	Depth	8
		Heads	16
		Embedding dims	512
Matching decoder	Dual-stream (ours)	Depth	8
		Heads	1
		Embedding dims	256
<b>UniCorrn (large)</b>			
Image backbone	ViT-L [17]	Depth	24
		Heads	16
		Embedding dims	1024
Point cloud backbone	PTv3 [72]	Depth	[3, 6, 6]
		Heads	[2, 8, 32]
		Embedding dims	[32, 128, 512]
Feature fusion encoder	Cross-view [69]	Depth	12
		Heads	16
		Embedding dims	768
Matching decoder	Dual-stream (ours)	Depth	8
		Heads	1
		Embedding dims	256

Table 12. **Hyper-parameters** for large-scale stage 1 and stage 2 training.

Hyperparameters	Stage 1	Stage 2
Tasks	2D-2D, 3D-3D	2D-2D, 2D-3D, 3D-3D
Optimizer	AdamW [38]	AdamW [38]
Base learning rate	1e-4	2e-5
Minimum learning rate	1e-7	1e-7
Weight decay	0.01	0.01
Adam $\beta$	(0.9, 0.95)	(0.9, 0.95)
Batch size (per task)	24	16
Epochs	40	30
Warmup epochs	4	5
Learning rate scheduler	Cosine decay	Cosine decay
Gradient norm clipping	1.0	1.0
Pre-trained weights	CroCo V2 [69]	Ours (Stage 1)

Table 13. Dataset sample sizes for large-scale training.

Dataset	Type	Pairs per epoch
<b>2D-2D (stage 1)</b>		
ArkitScenes [2]	Indoor / Real	45,600
BlendedMVS [76]	Mixed / Synthetic	68,400
CO3Dv2 [49]	Object-centric / Real	22,800
MegaDepth [36]	Outdoor / Real	68,400
Static Things 3D [42]	Object / Synthetic	22,800
ScanNet++ [77]	Indoor / Real	60,000
Waymo [56]	Outdoor / Real	60,000
<b>3D-3D (stage 1)</b>		
3DMatch [83]	Indoor / Real	20,586
ModelNet [73]	Object-centric / Synthetic	5,112
ArkitScenes [2]	Indoor / Real	80,000
MegaDepth [36]	Outdoor / Real	80,000
ScanNet++ [77]	Indoor / Real	80,000
<b>2D-2D (stage 2)</b>		
MegaDepth [36]	Outdoor / Real	20,000
ScanNet++ [77]	Indoor / Real	20,000
<b>2D-3D (stage 2)</b>		
7Scenes [21]	Indoor / Real	4,048
RGB-D Scenes V2 [30]	Indoor / Real	1,748
ScanNet++ [77]	Indoor / Real	10,000
<b>3D-3D (stage 2)</b>		
3DMatch [83]	Indoor / Real	20,586
ModelNet [73]	Object-centric / Synthetic	5,112
ArkitScenes [2]	Indoor / Real	10,000
ScanNet++ [77]	Indoor / Real	20,000

Table 14. Evaluation results on RGB-D Scenes V2 [30]. **Boldfaced** numbers highlight the best and the second best are underlined.

Model	Scene-11	Scene-12	Scene-13	Scene-14	Mean
Mean depth (m)	1.74	1.66	1.18	1.39	1.49
<i>Inlier Ratio(IR) <math>\uparrow</math></i>					
FCGF-2D3D [9]	6.8	8.5	11.8	5.4	8.1
P2-Net [63]	9.7	12.8	17.0	9.3	12.2
Predator-2D3D [25]	17.7	19.4	17.2	8.4	15.7
2D3D-MATR [33]	32.8	34.4	39.2	23.3	32.4
B2-3Dnet [8]	36.4	32.7	<u>43.8</u>	<u>27.4</u>	<u>35.1</u>
FreeReg [64]	<u>36.6</u>	<u>34.5</u>	34.2	18.2	30.9
<b>Ours (stage 2)</b>	<b>85.7</b>	<b>86.7</b>	<b>92.5</b>	<b>69.1</b>	<b>83.6</b>
<i>Feature Matching Recall (FMR) <math>\uparrow</math></i>					
FCGF-2D3D [9]	11.1	30.4	51.5	15.5	27.1
P2-Net [63]	48.6	65.7	82.5	41.6	59.6
Predator-2D3D [25]	86.1	89.2	63.9	24.3	65.9
2D3D-MATR [33]	<u>98.6</u>	<u>98.0</u>	88.7	77.9	90.8
B2-3Dnet [8]	<b>100.0</b>	<b>99.0</b>	92.8	85.8	94.4
FreeReg [64]	91.9	93.4	93.1	49.6	82.0
<b>Ours (stage 2)</b>	<u>98.6</u>	97.2	<b>100.0</b>	<b>92.0</b>	<b>97.0</b>
<i>Registration Recall (RR) <math>\uparrow</math></i>					
FCGF-2D3D [9]	26.4	41.2	37.1	16.8	30.4
P2-Net [63]	40.3	40.2	41.2	31.9	38.4
Predator-2D3D [25]	44.4	41.2	21.6	13.7	30.2
2D3D-MATR [33]	63.9	53.9	58.8	49.1	56.4
B2-3Dnet [8]	58.3	60.8	74.2	60.2	63.4
FreeReg [64]	74.2	72.5	54.5	27.9	57.3
Diff-Reg [71]	95.8	<b>96.1</b>	88.7	69.0	87.4
<b>Ours (stage 2)</b>	<b>98.6</b>	<u>95.3</u>	<b>99.0</b>	<b>76.9</b>	<b>92.5</b>

Table 15. Evaluation results on 7Scenes [21]. **Boldfaced** numbers highlight the best and the second best are underlined.

Model	Chess	Fire	Heads	Office	Pumpkin	Kitchen	Stairs	Mean
Mean depth (m)	1.78	1.55	0.80	2.03	2.25	2.13	1.84	1.77
<i>Inlier Ratio (IR) ↑</i>								
FCGF-2D3D [9]	34.2	32.8	14.8	26.0	23.3	22.5	6.0	22.8
P2-Net [63]	55.2	46.7	13.0	36.2	32.0	32.8	5.8	31.7
Predator-2D3D [25]	34.7	33.8	16.6	25.9	23.1	22.2	7.5	23.4
2D3D-MATR [33]	72.1	66.0	31.3	60.7	50.2	52.5	18.1	50.1
B2-3Dnet [8]	73.8	66.7	33.1	61.7	50.8	52.3	18.1	50.9
Diff-Reg [71]	79.2	71.0	54.1	70.4	55.8	60.2	22.9	59.1
Ours (stage 2)	<b>93.7</b>	<b>91.2</b>	<b>92.3</b>	<b>94.8</b>	<b>80.5</b>	<b>87.3</b>	<b>36.7</b>	<b>82.4</b>
<i>Feature Matching Recall (FMR) ↑</i>								
FCGF-2D3D [9]	99.7	98.2	69.9	97.1	83.0	87.7	16.2	78.8
P2-Net [63]	<b>100.0</b>	99.3	58.9	99.1	87.2	92.2	16.2	79.0
Predator-2D3D [25]	91.3	95.1	76.7	88.6	79.2	80.6	31.1	77.5
2D3D-MATR [33]	<b>100.0</b>	<u>99.6</u>	<u>98.6</u>	<b>100.0</b>	<u>92.4</u>	95.9	58.1	92.1
B2-3Dnet [8]	<b>100.0</b>	<b>100.0</b>	<u>98.6</u>	<b>100.0</b>	<b>92.7</b>	95.6	<b>64.9</b>	<b>93.1</b>
Diff-Reg [71]	<b>100.0</b>	<b>100.0</b>	<b>100.0</b>	<b>100.0</b>	91.3	<u>98.1</u>	58.1	92.5
Ours (stage 2)	<b>100.0</b>	<b>100.0</b>	<b>100.0</b>	<b>100.0</b>	90.5	<b>99.9</b>	<u>60.7</u>	<u>93.0</u>
<i>Registration Recall (RR) ↑</i>								
FCGF-2D3D [9]	89.5	79.7	19.2	85.9	69.4	79.0	6.8	61.4
P2-Net [63]	96.9	86.5	20.5	91.7	75.3	85.2	4.1	65.7
Predator-2D3D [25]	69.6	60.7	17.8	62.9	56.2	62.6	9.5	48.5
2D3D-MATR [33]	96.9	90.7	52.1	95.5	80.9	86.1	28.4	75.8
B2-3Dnet [8]	98.3	90.5	56.2	96.4	84.0	86.1	<u>32.4</u>	77.7
Diff-Reg [71]	<b>100.0</b>	<u>94.0</u>	<u>90.4</u>	<u>99.3</u>	81.2	<u>94.6</u>	27.0	<u>83.8</u>
Ours (stage 2)	<b>100.0</b>	<b>99.3</b>	<b>98.6</b>	<b>100.0</b>	<b>88.8</b>	<b>98.5</b>	<b>51.9</b>	<b>91.0</b>